AGU PUBLICATIONS

JGR

Journal of Geophysical Research: Solid Earth

RESEARCH ARTICLE
10.1002/2014JB011611

Key Points:
- Delayed and frequency-dependent triggering observed in lab friction experiments
- Rate-state models predict either stressing rate- or duration-limited triggering
- Faults may heal more slowly and be more susceptible to triggering than thought

Correspondence to:
N. J. van der Elst,
nicholas@ldeo.columbia.edu

Citation:
van der Elst, N. J., and H. M. Savage (2015), Frequency dependence of delayed and instantaneous triggering on laboratory and simulated faults governed by rate-state friction, *J. Geophys. Res. Solid Earth*, *120*, 3406–3429, doi:10.1002/2014JB011611.

Received 17 SEP 2014
Accepted 14 APR 2015
Accepted article online 21 APR 2015
Published online 23 MAY 2015

Frequency dependence of delayed and instantaneous triggering on laboratory and simulated faults governed by rate-state friction

Nicholas J. van der Elst[1] and Heather M. Savage[1]

[1]Lamont-Doherty Earth Observatory, Columbia University, Palisades, New York, USA

Abstract Earthquake triggering by transient stresses is commonly observed; however, some aspects remain unexplained. The first is the often-observed delay between the triggered earthquakes and the triggering waves, and the second is the unexpected effectiveness of transient stressing in the seismic frequency band. Previous theoretical and laboratory studies have suggested that seismic transients should have little impact on faults if the duration of the transient is smaller than the timescale for nucleation of slip. We reexamine the dynamics of stress triggering during stick-slip sliding on a laboratory fault and make three important observations that pertain to earthquake triggering. (1) Delayed triggering (clock advance) occurs for both bare granite surfaces and granular gouge prior to the onset of instantaneous triggering. (2) Triggering occurs much earlier in the stick-slip cycle than expected for a simple Coulomb stress threshold. (3) Shorter-period (higher stressing rate) pulses are more effective at triggering than longer-period pulses of the same stress amplitude. We use numerical simulations to show that rate-state friction can explain each of the observed features but not all three simultaneously. Only the Ruina slip law for state evolution, in which faults must slip to heal, can reproduce early-onset and stressing rate-dependent triggering. The laboratory and numerical experiments show that faults can remain relatively weak over much of the seismic cycle and that the triggered response depends on a competition between healing and weakening during triggered slip. Transient stressing at seismic frequencies may be more effective at triggering earthquakes than previously recognized.

1. Introduction

Dynamic earthquake triggering, where earthquakes are set off by transient perturbations such as tides or passing seismic waves from other distant earthquakes, is a robustly observed phenomenon [*Brodsky et al.*, 2000; *Brodsky and Prejean*, 2005; *Cochran et al.*, 2004; *Fischer et al.*, 2008; *Gomberg and Davis*, 1996; *Gomberg and Johnson*, 2005; *Gomberg et al.*, 2001; *Hill and Prejean*, 2007; *Hill et al.*, 1993; *Husker and Brodsky*, 2004; *Métivier et al.*, 2009; *Peng et al.*, 2010; *Pollitz et al.*, 2012; *Prejean et al.*, 2004; *Rubinstein et al.*, 2011; *van der Elst and Brodsky*, 2010; *Velasco et al.*, 2008; *Wu et al.*, 2011]. Earthquake triggering is more prevalent in certain regions, such as volcanic and geothermal areas, but is demonstrably a global phenomenon [*Velasco et al.*, 2008]. While most studies focus on remote events, dynamic triggering may also be important for triggering aftershocks in the near field of a mainshock [*Felzer and Brodsky*, 2006; *Gomberg et al.*, 2003; *van der Elst and Brodsky*, 2010]. On occasion, triggered earthquakes can be large, with $M_W > 6$ events recently documented [*Pollitz et al.*, 2012]. Other fault slip phenomena such as tectonic tremor appear even more susceptible to triggering than conventional earthquakes.

In addition to causing other potentially significant earthquakes, triggering is a useful tool, in that it informs us about in situ stress on the fault, and may indicate when a fault is reaching a critical state [*Brodsky and van der Elst*, 2014; *van der Elst et al.*, 2013]. In a simple Coulomb friction framework, a critically stressed fault is one on which the load has built up over time to approach some fixed frictional strength. In the more modern context of rate-state friction, however, frictional strength is dependent on both sliding rate and sliding history (state) [*Dieterich*, 1994; *Dieterich*, 1979; *Marone*, 1998], and the concept of a critically stressed fault grows fuzzier. In a rate-state framework, criticality (proximity to failure) is determined by a competition between loading and healing, with very different implications for susceptibility to triggering throughout the cycle.

Historically, considerations of the rate- and state-dependent nature of fault friction have led to the conclusion that higher-frequency (shorter-period) stress transients should be relatively ineffective at triggering earthquakes, because fault friction does not have time to evolve at timescales shorter than some intrinsic nucleation time [*Dieterich*, 1987, 1992; *Scholz*, 2003]. This nucleation time is thought to be on the order of a year, based on laboratory observations [*Beeler and Lockner*, 2003] and studies of aftershock sequence duration [*Dieterich*, 1994]. This timescale has been used to explain the poor correlation between earthquakes and tides [*Beeler and Lockner*, 2003], and has also been thought to limit the importance of the peak transient stresses with respect to aftershock triggering in the near field [*Scholz*, 1998]. If faults are insensitive to tides, they should be similarly insensitive to dynamic stressing at seismic periods.

Another observed feature of dynamic triggering that still requires explanation is delayed triggering, in which the onset of the triggered earthquakes is delayed with respect to the passage of the transient stress, requiring that the triggering process lasts longer than the transient itself [*Brodsky*, 2006; *Brodsky and Prejean*, 2005]. Several ideas have been put forward to explain the delayed onset in terms of secondary triggering mechanisms, including cascades of triggered seismicity [*Brodsky*, 2006], aseismic slip that loads secondary faults [*Hill and Prejean*, 2007; *Shelly et al.*, 2011], and triggered changes to fault hydrology and permeability [*Brodsky et al.*, 2003; *Elkhoury et al.*, 2006, 2011]. However, delayed triggering is also possible within the context of rate and state friction [*Gomberg et al.*, 1997; *Perfettini et al.*, 2003]. If the transient stress leads to evolution of the frictional state by renewal of frictional contacts, this can advance the fault along the path to failure and lead to delayed triggering through "clock advance."

Here we report on laboratory experiments that investigate the response of a frictional interface to pulse-like transients during stick-slip sliding. These experiments were first described by *Savage and Marone* [2008] and treat both bare granite surfaces and layers of granular gouge. In this new analysis, we revisit the experiments for two reasons. First, we reexamine the results for delayed triggering and clock advance, to establish whether this phenomenon can arise from rate-state frictional dynamics. Second, *Savage and Marone* [2008] identified an effect of oscillation frequency on triggered slip, for oscillations with periods shorter than the nucleation time. We revisit this frequency dependence here, both with a more complete analysis of the experiments and with a greatly expanded suite of numerical simulations that map out the full range of behaviors possible under the rate-state friction model. We map out the onset of triggering—defined as the time at which the system becomes susceptible to instantaneous or delayed triggering—as a function of frequency, amplitude, and duration of the transient. We go on to describe different modes of triggering allowed by the rate-state friction model and show where the model agrees with the lab experiments. Finally, we discuss some remaining discrepancies between the model and the experiments, and lay out the implications of our study for the concept of critically loaded faults in nature and dynamic triggering of earthquakes.

1.1. Earthquake Triggering and Rate-State Friction Laws

Rate and state friction dynamics have been explored through both analytical and numerical treatment of an elastically coupled spring and slider block [e.g., *Gomberg et al.*, 1998; *Gu et al.*, 1984; *Rice and Ruina*, 1983]. We briefly summarize the major features of the model here. In rate-state friction, the frictional strength τ is proportional to the normal stress σ and is also related to the current sliding velocity v and the history of sliding through the state variable θ;

$$\tau = \tau_* + a\sigma \ln \frac{v}{v_*} + b\sigma \ln \frac{\theta}{\theta_*}. \tag{1}$$

Parameter a is the "direct-effect" coefficient that governs the instantaneous strengthening in response to a velocity increase, and parameter b governs the rate of healing of frictional contacts. Rate-state friction is defined relative to a reference stress $\tau_*(v_*, \theta_*)$. The frictional interface is coupled elastically to a load point:

$$\dot{\tau} = k\left(v_{\mathrm{lp}} - v\right), \tag{2}$$

where k is the elastic stiffness and v_{lp} is the load point velocity.

The state is most commonly assumed to evolve according to one of two equations:

$$\dot{\theta} = 1 - \frac{\theta v}{d_c}, \tag{3a}$$

$$\dot{\theta} = -\frac{\theta v}{d_c} \ln\left(\frac{\theta v}{d_c}\right). \tag{3b}$$

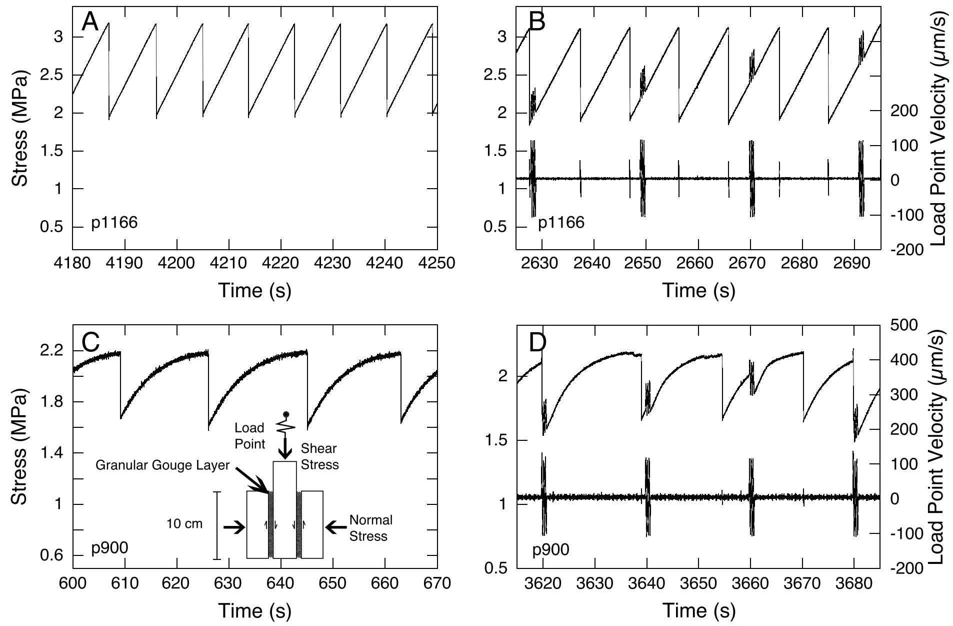

Figure 1. Samples are loaded with 5 MPa normal stress σ and a constant vertical displacement rate v_{lp} of 5 μm/s. Under constant displacement rate, stick-slip failures occur at very regular intervals, for (a) granite surfaces and (c) glass beads. Samples consist of either two layers of glass beads sandwiched between steel forcing blocks (inset in Figure 1c) or bare granite surfaces. When introduced into the vertical load path (b, granite surfaces; d, glass beads), the transient causes immediate failure (instantaneous triggering), has no effect, or advances the timing of the subsequent slip event (delayed triggering).

In the Dieterich "aging" law (3a), the fault heals during truly stationary contact, and the state has the interpretation of the average contact lifetime of microscopic asperities on the frictional interface [*Dieterich and Conrad*, 1984]. In the Ruina "slip" law (3b), state can only evolve during sliding [*Ruina*, 1983]. [The designation of equation (3a) as the "Dieterich" law and equation (3b) as the "Ruina" law is a matter of convenience.] These two formulations predict almost identical behavior near steady state but predict substantially different healing rates early in the stick-slip cycle. For both equations, there is a sign change (from healing to weakening) when $\theta v = d_c$. This is a crucial point for determining the response to transient oscillations.

1.1.1. Rate-State Timescales and the Response to Transients in Previous Experiments

The dynamical equations (1)–(3) contain several timescales that govern the response of a fault to a transient of a given frequency or duration. The most well known is the timescale for nucleation, identified by [*Dieterich*, 1992]:

$$t_n = \frac{a\sigma}{\dot{\tau}}, \tag{4}$$

where $\dot{\tau} = k v_{lp}$ is the stressing rate. *Beeler and Lockner* [2003] analyzed a laboratory fault subjected to continuous load oscillations and found that the peak rate of stick-slip events correlated with the peak transient stressing rate, as long as the oscillation period was longer than the nucleation timescale. For periods shorter than the nucleation timescale, events occurred in phase with the peak stress. Importantly, the stress amplitude threshold for correlated slip at periods shorter than the nucleation timescale was greater than that predicted by a simple Coulomb law (where failure occurs if and only if the transient stress exceeds a simple friction threshold). One of the key conclusions of these experiments is that the triggering potential of a transient pulse diminishes at periods shorter than the nucleation timescale.

The nucleation timescale [equation (4)] describes the time from the initiation of nucleation to fully unstable slip. Another potentially important timescale for dynamic triggering is the natural oscillation period of the stably sliding spring-slider system. When a spring-slider is loaded at critical stiffness—that is, precisely on the boundary between stable and unstable slip [*Gu et al.*, 1984]—slip speed will oscillate harmonically about the load point velocity in response to a small perturbation. The period of this oscillation is the natural period of the spring-slider T_c [*Rice and Ruina*, 1983], where

$$T_c = 2\pi\sqrt{a/(b-a)}d_c/v_{lp}. \tag{5}$$

Transient forcing at periods similar to T_c may have a relatively large effect on the fault, just as forcing at the resonant frequency of an oscillator produces a maximal effect. The response of the fault to oscillations shorter than T_c, on the other hand, may be damped. Numerical studies on stably sliding faults have confirmed this expectation [*Perfettini and Schmittbuhl*, 2001; *Ader et al.*, 2012]. *Boettcher and Marone* [2004] and *Savage and Marone* [2007] experimentally confirmed a transition in frictional response at forcing periods similar to d_c/v_{lp}, for normal stress oscillations on stably sliding faults and shear stress oscillations on stick-slip sliding faults, respectively. While the triggered response was well modeled at periods longer than the T_c, the response was less well modeled at shorter periods [*Boettcher and Marone*, 2004]. Since these are the periods representative of forcing by seismic waves, further investigation is warranted.

Our study more thoroughly investigates transient triggering than previous work in two ways. The first is that we use pulse-like transients to simulate dynamic triggering by seismic waves. Continuous oscillations will obscure any frictional responses that take longer than the duration of the transient to emerge, and cannot be sensitive to delayed triggering. Second, all of the previous studies compared the experimental observations to predictions of rate-state friction over a relatively limited range of friction parameters, determined from steady sliding tests at a narrow range of velocities. Recent studies show significant evolution of the rate-state parameters with displacement and slip velocity [e.g., *Ikari et al.*, 2011, 2013], leaving open the possibility that frictional parameters measured for steady sliding may not be appropriate for modeling the entire stick-slip cycle. In this study, we run an extensive suite of simulations, for a wide range of friction parameters, to map out all of the possible modes of triggering slip behavior under the rate-state friction framework. This allows us to identify whole model spaces that show very different behavior than previously documented.

2. Methods

2.1. Lab Experiments

The experiments were conducted in a servo-controlled biaxial deformation apparatus at Penn State University. The sample is loaded in a double-direct shear configuration (Figure 1c inset). In this configuration, samples consist of either two 3 mm thick gouge layers, sandwiched between two steel side blocks and a center forcing block, or three granite blocks in the same configuration. Bare granite surfaces are roughened with 150 grit polish and cleaned with methanol before each experiment. For the gouge experiments, we use soda lime glass beads (105–149 μm diameter) to simulate granular fault gouge. Glass beads and granite surfaces are ideal materials to use for these experiments because they fail in unstable stick slip with very regular recurrence intervals under constant displacement rate (Figures 1a and 1c). Normal stress is held constant at 5 MPa, and shear displacement is driven at 5 μm/s. Under such low normal loads, there is little grain breakage or comminution and we avoid evolution of the stick-slip recurrence time over the course of the experiments. For more details on these experiments, see *Savage and Marone* [2008].

We model a transient seismic wave as a load point velocity oscillation of the form $v'(t) = Af\sin(2\pi ft)$, with amplitude $A > 0$ and frequency f. The stress transmitted to the fault is proportional to the integral of the velocity oscillation: $\tau'(t) = A\frac{1}{2\pi}[1-\cos(2\pi ft)]$. Note that this defines a positive-only stress transient, while the transient load in a real seismic wave will be both positive and negative. Simulations show that rate-state faults are relatively insensitive to the negative phase of the pulse, and the two types of transients produce essentially the same fault response. We define a single stress "pulse" as one complete velocity sinusoid, which returns the transient stress to zero. The prefactor A is scaled with frequency so that the peak stress amplitude is constant with respect to frequency, while the peak stressing rate varies. We systematically vary the transient amplitude, frequency, and duration to assess the effect on instantaneous and delayed triggering (Table 1). The oscillations recur at a slightly longer period than the stick-slip cycle so that the time between the last stick slip and the transient varies (Figures 1b and 1d), and each cycle is perturbed by no more than a single transient. The ratio of transient stress amplitude to the stress

Table 1. List of Experiments

Experiment	Layer Thickness (mm)	Amplitude (μm/s)	Frequency (Hz)	Experiment Type
p852	3	15, 30, 40, 60	1	1 s duration[a]
p900	3	30, 40, 60, 80, 120	1, 1, 1, 2, 3	1 s duration
p908	3	30, 40, 60, 80	1, 1,2, 3	1 s duration
p923	3	40, 80, 120	1, 2, 3	Single pulse
p937	3	40, 80, 120	1, 2, 3	Single pulse
p997	3	3, 5, 10, 15	1	1 s duration
p1145	3	20, 60	1	1 s duration
p1165	3	40, 80, 120, 160	1, 2, 3, 4	1 s duration
p1166	Smooth	35, 40, 80, 120, 160	1, 2, 3, 4	1 s duration, single pulse
p1172	Smooth	40, 80, 120, 160	1, 2, 3, 4	1 s duration, single pulse
p1173	Smooth	40, 80, 120, 160	1, 2, 3, 4	1 s duration, single pulse
p1178	Smooth	5, 10, 30, 40, 50	1	1 s duration
p1227	Smooth	5, 40, 80, 120, 160	1, 2, 3, 4	1 s duration

[a]Number of pulses proportional to frequency to give constant duration.

change during the stick-slip cycle in these experiments is much larger than those of tides and seismic waves from remote earthquakes in nature, and is on the order of seismic waves in the near field. Such large amplitudes are used to ensure a measurable response, relative to the natural variability of the recurrence intervals.

The timing of the transient and the timing of the subsequent slip event are measured with respect to the termination of the previous slip event and normalized by the average recurrence time for an unperturbed cycle (Figure 2). Failure that occurs during the transient itself is called *instantaneous* triggering, and failure that occurs after the transient, but earlier than the average unperturbed recurrence interval, is called *delayed* triggering. The *onset* of triggering is defined as the earliest time within the cycle at which either form of triggering is detectable. We set the threshold for identifying delayed triggering at 1 standard deviation below the mean recurrence time, here equal to a clock advance of 2.5%.

The present study improves upon the analysis of *Savage and Marone* [2008] by carefully normalizing the triggered failure time by the average unperturbed recurrence time in each experimental run. This improves the precision relative to the previous analysis, which normalized the triggered failure times by the average unperturbed recurrence over all experiments.

2.2. Numerical Experiments

We model the frictional behavior by solving the system of equations in (1)–(3), treating the experimental apparatus as a spring and slider-block system [*Rice and Ruina*, 1983; *Gomberg et al.*, 1997; *Belardinelli et al.*, 2003; and many others]. While we attempt to scale the results to earthquake timescales, we focus on reproducing the experimental observations and do not explicitly attempt to model realistic seismic waves impinging on a 2-D fault. We save the full description of the numerical model until after the presentation of the laboratory results.

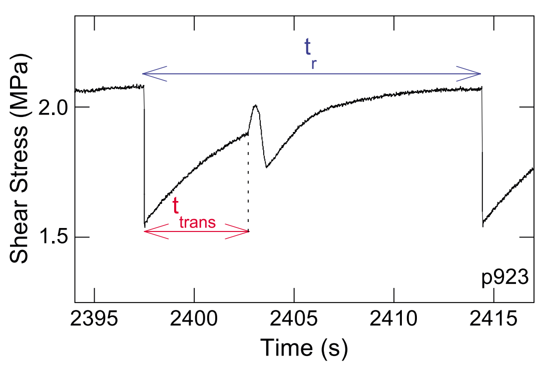

Figure 2. Recurrence time is measured as the time between two concurrent stick-slip events. The timing of the transient in the stick-slip cycle is measured from the time of the last stick slip to the start of the transient pulse. Both of these values are normalized by average baseline recurrence times and are referred to as normalized failure time and normalized trigger time, respectively.

3. Results

We present the results of the laboratory experiments with a special focus on the effect of transient frequency and duration, in order to establish the important features that should be reproduced by the rate-state simulations. As a baseline for the discussion, we compare the onset of triggering in the experiments to a simple Coulomb model of friction, in which triggering occurs only if the stress during the transient

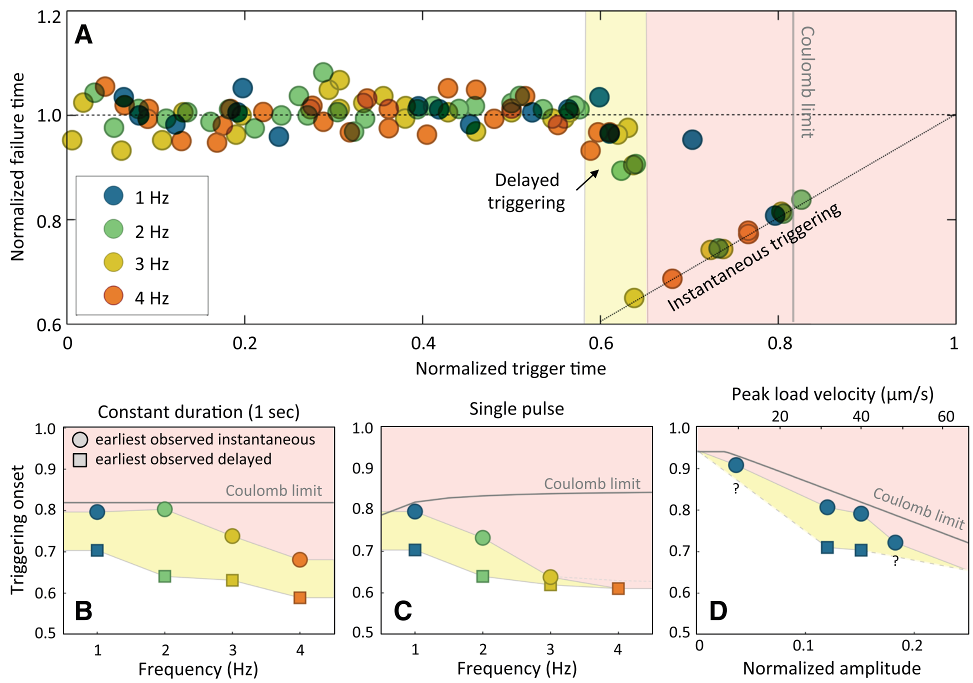

Figure 3. Experimentally observed triggering on bare granite surfaces. (a) Normalized failure time as a function of the timing of the trigger within the stick-slip cycle. Instantaneous triggering (shaded in red) follows the 1:1 line. Delayed triggering (clock advance) is inferred where points fall below the horizontal baseline but above the 1:1 line (shaded in yellow). The Coulomb limit marks the point where triggering would be expected for a simple Coulomb threshold. (b) Onset of triggering as a function of frequency for constant-duration (1 s) transients. (c) Onset of triggering as a function of frequency for single-pulse transients. The Coulomb limit is later for shorter pulses because there is less contribution from background loading. (d) Onset of triggering as a function of transient amplitude (normalized by stress drop in the unperturbed cycle) for 1 Hz single-pulse transients. Not all experiments sampled the seismic cycle continuously enough to capture the onset of delayed triggering.

exceeds the frictional strength measured in unperturbed experiments (e.g., the Coulomb triggering onset is at 90% of the cycle time for a stress transient that is 10% of the cycle stress drop). We then turn to the rate-state simulations and search for behavior similar to that observed in the experiments, for various state evolution models and parameter ranges. In both sections, we report on the normalized onset time of triggering, the effects of transient frequency and duration, and the presence or absence of delayed triggering.

3.1. Triggering on Laboratory Faults

3.1.1. Bare Granite Surfaces

The experiments show that a certain amount of loading must occur before the transient stress triggers a change in the recurrence interval. Figure 3a shows the stick-slip recurrence time as a function of the timing of the trigger within the seismic cycle, both normalized by the unperturbed recurrence time. Delayed triggering begins at about 60% of the cycle, prior to the onset of instantaneous triggering at no more than 70% of the cycle. The peak stress in the transient pulse is only about 15% of the cycle stress drop. Triggering onset is therefore much earlier than would be expected for a Coulomb triggering model with a simple stress threshold.

There is a strong frequency dependence to the onset of triggering (Figure 3b); higher-frequency pulses result in an earlier onset of both instantaneous and delayed triggering. The granite surfaces subjected to a 1 Hz, 1 s pulse show the onset of delayed triggering at about 70% of the cycle and the onset of instantaneous triggering at 70–80% of the cycle (Figure 3b). At higher frequencies, both instantaneous triggering and delayed triggering arise much earlier in the cycle. For 4 Hz transients, instantaneous triggering is observed as early as 65% into the cycle (~20% earlier than expected based on the Coulomb friction model) and delayed triggering emerges as early as 60% into the cycle (Figures 3b and 3c). The frequency dependence holds not only for constant-duration transients, in which higher-frequency transients consist of multiple

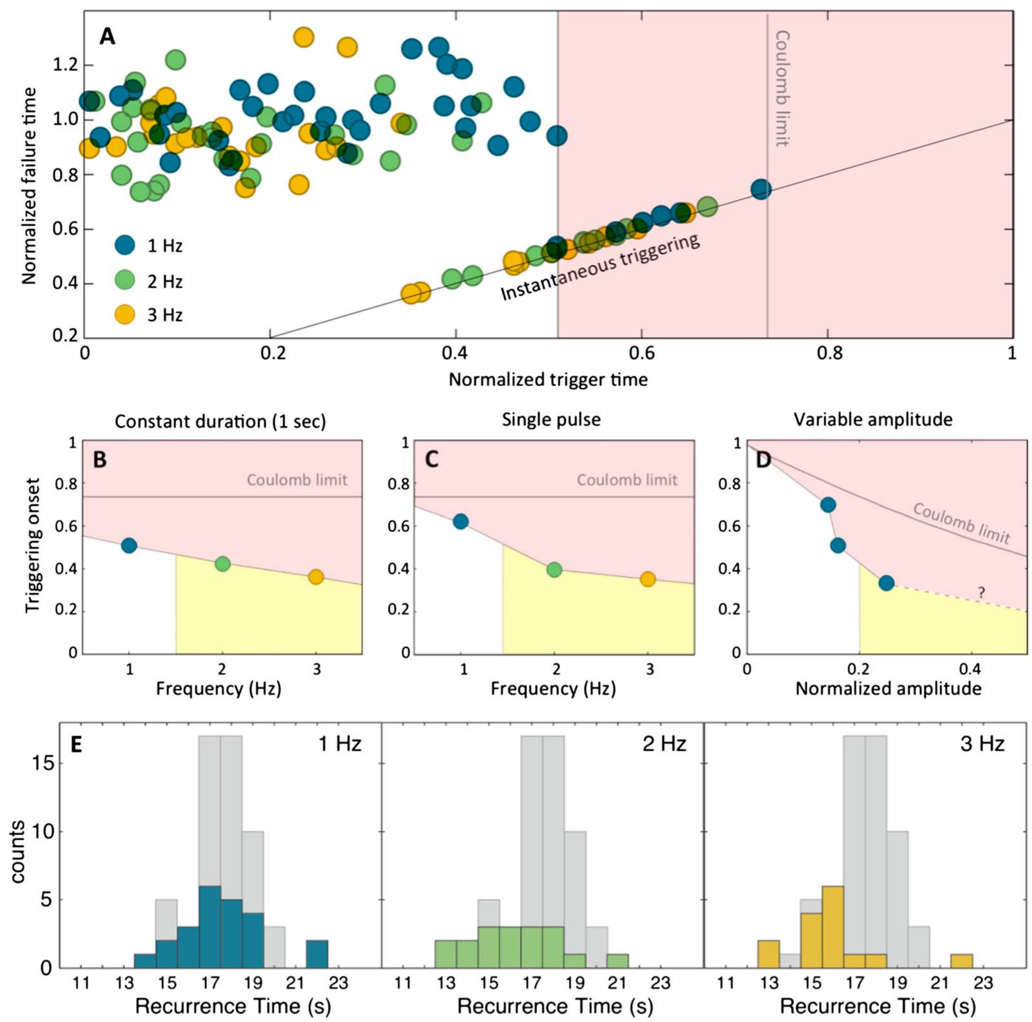

Figure 4. Recurrence time for stick slip on granular gouge consisting of glass beads subjected to transient oscillations. (a) Normalized recurrence time as a function of transient timing within the stick-slip cycle. The portion of the cycle where instantaneous triggering occurs for a 1 Hz pulse is shaded in red. (b) Onset of instantaneous triggering as a function of frequency for constant-duration (1 s) transients. Circles mark the earliest observed instance of instantaneous triggering. (c) Triggering onset for single-pulse experiments. (d) Onset as a function of transient amplitude (1 Hz, 1 s pulses). (E) Histograms of recurrence time vs. transient frequency, for cases that do not result in instantaneous triggering. Gray bars show distribution of unperturbed recurrence times. Clock advance is frequency dependent ($p = 0.80$, 0.005, and 0.0004, by the Chi-squared test for 1, 2, and 3 Hz, respectively).

pulses, but also for single pulses where higher-frequency pulses have proportionately shorter durations (Figure 3c). The onset of instantaneous triggering is also a function of transient amplitude, with larger amplitudes driving triggering earlier in the cycle (Figure 3d).

The reported triggering onsets are for the earliest observation of instantaneous or delayed triggering under each experimental condition. The delayed triggering onset may therefore be as early as the last untriggered point, and the instantaneous onset may be as early as the last delayed-triggered point. The reported onsets are therefore upper bounds.

3.1.2. Granular Gouge Experiments

The granular gouge has a response similar to that of the bare granite surfaces but with some important differences (Figure 4). The first important difference is that the loading curve during the inter-seismic period is highly nonlinear, with a strong rollover at the end of the cycle that cannot be reproduced by a simple linear-elastic or rate-state slider model (Figure 1c). Nevertheless, the onset of instantaneous triggering follows a similar trend as for the granite surfaces.

Table 2. Model Parameters

v_{lp} (μm/s)	σ_n (MPa)	$\Delta\tau$ (MPa)	t_r (s)	$\Delta\tau'$ (MPa)	k (MPa/μm)	μ_*	d_c (μm)	a	b
5	5	1.82	16.9	0.27	0.0215	0.65	1–3	0.001–0.05	0.013–0.062

The onset of instantaneous triggering in the granular gouge is dependent on the frequency of the transients, with higher-frequency (3 Hz) transients triggering failure at least 10% earlier in the cycle than lower-frequency (1 Hz) transients (Figures 4b and 4c). Just as observed for the granite blocks, the onset of instantaneous triggering does not depend on the duration of the transient (i.e., single or multiple pulses). The triggering onset is also sensitive to the stress amplitude, perhaps more so than predicted by a simple Coulomb model (Figure 4d).

Delayed triggering for the granular gouge differs somewhat from delayed triggering for the granite surfaces. Like the bare surface experiments, higher-frequency oscillations (2 and 3 Hz) give rise to a significantly shorter recurrence interval, as demonstrated by Student's *t*-test (Figure 4e). The probability that the perturbed recurrence times (excluding the instantaneously triggered subset) come from the same distribution as the set of unperturbed recurrence times is 0.004 and 0.0005 for 2 and 3 Hz pulses, respectively (with single-pulse and constant-duration experiments combined). However, contrary to the granite blocks, the clock advance does not depend on the timing of the transient within the cycle (Figure 4a). Instead, the stick-slip interval is 1–2 s shorter no matter how early the transient falls in the cycle. The highest amplitude oscillations also produce delayed triggering throughout the cycle (Figure 4d).

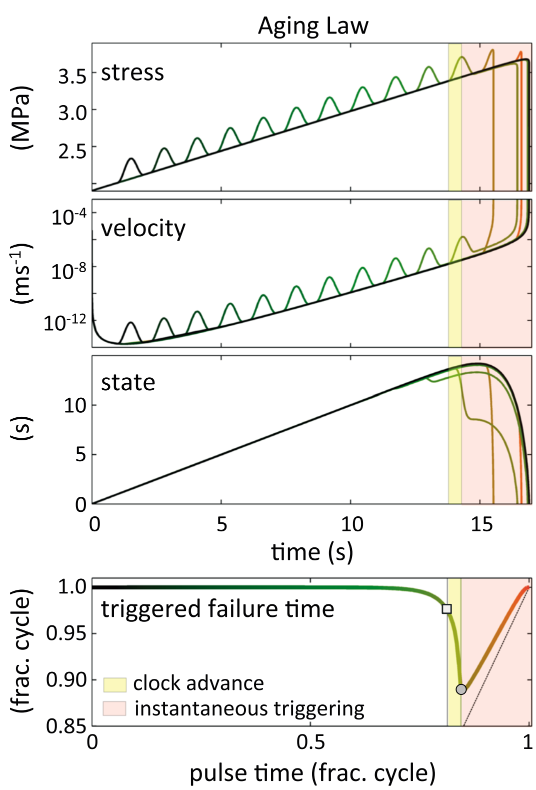

Figure 5. Example rate-state simulations with the Dieterich aging law [equation (3a)]. Multiple simulations are overlain, with a 1 s load pulse at different times throughout the cycle. Velocity is on a log scale. The bottom panel shows the triggered failure time as a function of the pulse time (normalized by the background recurrence time). Simulation parameters are $a = 0.015$, $b - a = 0.012$, $d_c = 1$ μm, and other parameters as in Table 2.

In summary, both the bare granite blocks and the granular gouge show triggering much earlier than expected for a simple Coulomb threshold, and triggering is a function of frequency and amplitude. Different frequency pulses differ only in the stressing rate of each pulse and the number of pulses in a given duration. Since there appears to be no difference between the experiments with single and multiple pulses at a given frequency, we conclude that higher stressing rate oscillations drive triggering earlier in the cycle for both media and, in the case of the granular gouge, drive delayed triggering throughout the cycle.

3.2. Numerical Experiments

We model the frictional behavior of a simulated fault via equations (1)–(3). While the rate-state friction equations may be used to model either bare surface friction or granular gouge, the granular experiments have nonlinear loading curves as a function of load point displacement, and the frictional dynamics likely depend on dilation and compaction processes, which we do not model here. The numerical experiments are thus best compared to the bare granite surface experiments. The stress transient is modeled as a sinusoidal forcing term added to the load point velocity at successively later points within the stick-slip cycle. Just as in the laboratory experiments, we measure the time of onset for instantaneous and delayed triggering, with a threshold clock advance of 2.5% for identifying delayed triggering.

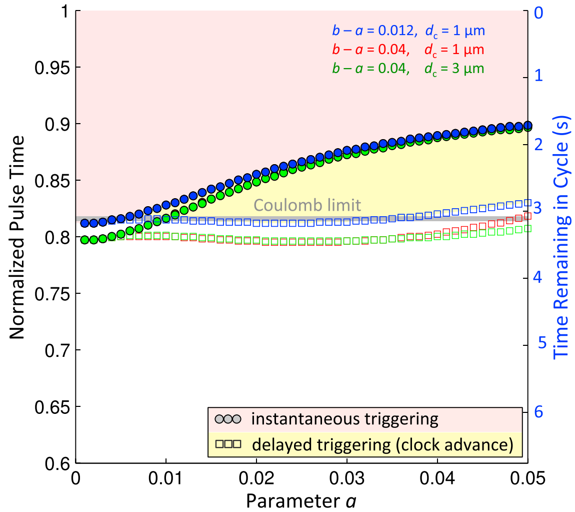

Figure 6. Onset of triggering for the Dieterich aging law [equation (3b)] as a function of the rate parameter a and other model parameters. Stress pulses that arrive earlier than the squares have negligible effect on recurrence time. Pulses that arrive between the squares and circles cause clock advance (yellow). Pulses that arrive later than the circles cause instantaneous triggering (red). The Coulomb limit (gray bar) is the point at which instantaneous triggering is expected for a simple Coulomb friction law. Shaded areas are for the model in blue; compare to Figure 5. The modeled stress pulse is a 1 s, 1 Hz sine pulse.

Model parameters such as loading stiffness and normal stress are set to match the experimental conditions (Table 2). We run simulations with a range of frictional parameters in order to explore the full range of behavior possible with the rate-state equations. However, we primarily use the critical slip distance $d_c = 1$ µm, estimated by *Savage and Marone* [2008], and vary the a and b parameters.

For each combination of frictional parameters a, b, and d_c, the unperturbed recurrence time of the stick-slip cycle is tuned to match the experiments through an appropriate choice of initial conditions (Appendix A). This is a crucial step, in that it ensures that the recurrence time and stress drop of the stick-slip cycle are constant, regardless of the chosen friction parameters. This provides consistency for analyzing the effects of transient duration and amplitude as a function of friction parameters.

3.2.1. Dieterich Aging Law

The evolution of stress, velocity, and state over the stick-slip cycle with Dieterich law state evolution [equation (3a)] is shown in Figure 5, for an example set of model parameters. The mechanism of triggering in the rate-state framework is evident in the evolution of the state variable during the transient. A complete reduction in state during the transient leads to instantaneous triggering, while a partial drop leads to delayed triggering.

For the Dieterich aging law [equation (3a)], the onset and style of triggering depends most strongly on the a parameter (Figure 6). This is to be expected, because a controls the instantaneous velocity response to the

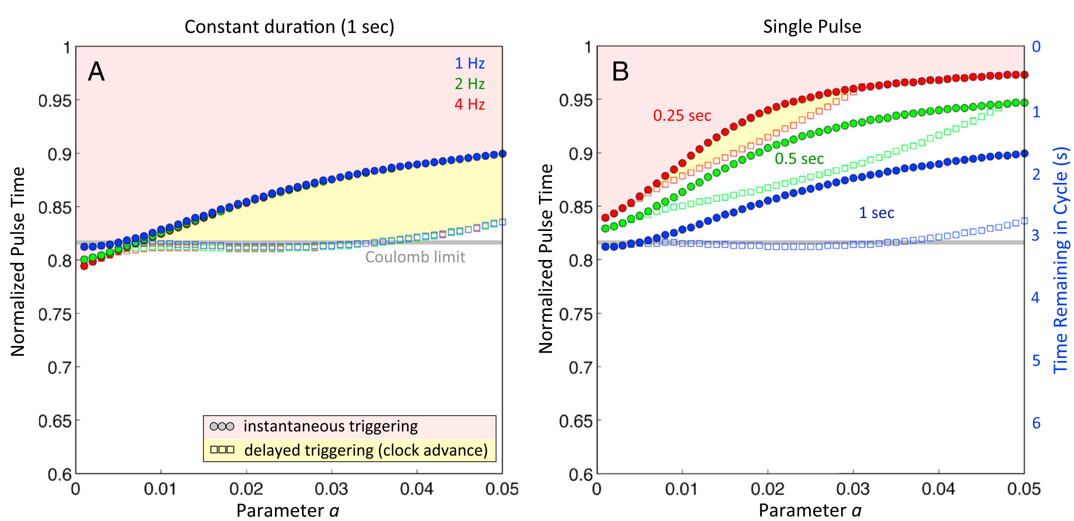

Figure 7. The effect of pulse frequency and duration for the Dieterich aging law [equation (3b)]. (a) Constant-duration transients of varying frequency. Pulses that arrive earlier than the squares have no effect on fault slip. Pulses that arrive between the squares and the circles cause clock advance (yellow). Pulses that arrive later than the circles cause instantaneous slip (red). The Coulomb limit (gray bar) is the point at which instantaneous triggering is expected for a simple Coulomb friction law. (b) Single pulse transients of varying duration. Shading is for 4 Hz, 0.25 s pulses. Model parameters: $b - a = 0.012$ and $d_c = 1$ µm.

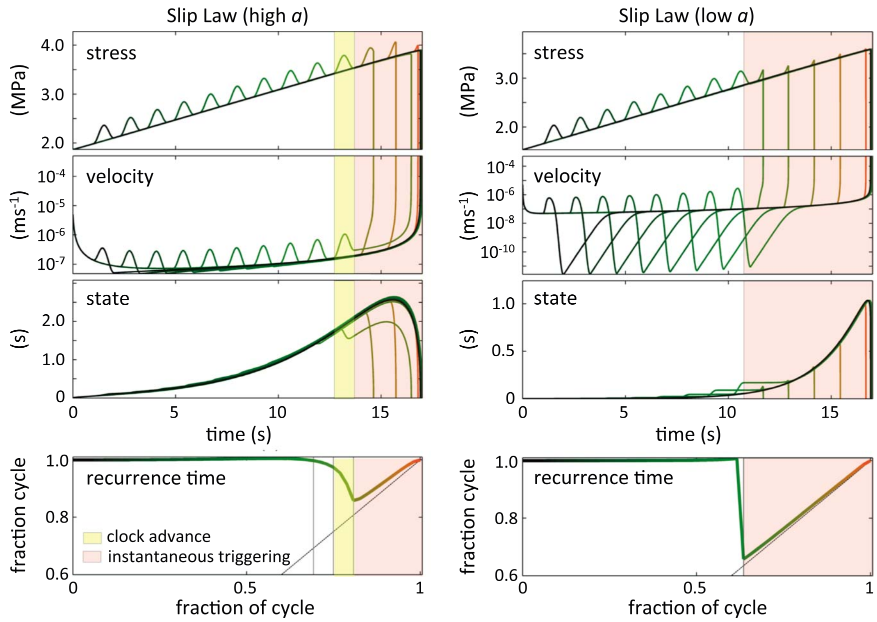

Figure 8. Example rate-state simulation using the Ruina law [equation (3b)]. Multiple simulations are overlain, with a 1 s load pulse at different times throughout the cycle. Velocity is on a log scale. The bottom panels show the triggered failure time as a function of the timing of the pulse (normalized by the background recurrence time). Simulation parameters are as follows: high $a = 0.04$, low $a = 0.005$, $b - a = 0.04$, and other parameters as in Table 2.

transient load [equation (1)]. As a increases, instantaneous triggering is pushed later in the cycle and appears to be replaced by delayed triggering. For large a (greater than about 0.011), the stress in the transient must significantly exceed the Coulomb threshold to trigger instantaneous slip.

The rate-weakening parameter $b - a$ influences the behavior only weakly; in general, there is negligibly earlier triggering onset for larger rate-weakening parameter (Figure 6). The critical displacement parameter d_c has virtually no impact on the triggering onset, which is somewhat surprising, given that it sets the minimum slip distance for fault weakening. This is explained by the way the recurrence interval is set to match the experimental observations. For the same initial conditions, changing d_c has a direct impact on the recurrence time for unstable slip. The initial conditions (initial stress) must therefore be changed along with d_c to match the observed recurrence time. This ultimately cancels out any stabilizing effect.

The Dieterich law predicts no dependence on frequency for transient pulses of the same duration (Figure 7a). The slight differences in triggering onset for small values of a (<0.005) are due to the fact that the constant-duration (multiple-pulse) transients sometimes trigger on the later stress peaks. This is a fairly small effect and is unable to explain the magnitude of the frequency dependence in the experimental observations. Furthermore, in our lab experiments, failure always occurs on the first pulse of a multi-pulse transient.

For single-pulse transients, where duration is inversely proportional to frequency, triggering onset arises later in the cycle for shorter-duration pulses for all values of a. The Dieterich model therefore predicts that higher-frequency, single-pulse transients should trigger substantially later in the cycle (Figure 7b), in disagreement with the observations.

3.2.2. Ruina Slip Law

The triggered slip response is significantly more complicated for the Ruina slip law [equation (3b)] than for the Dieterich aging law. The first major difference is that the fault remains relatively weak over the early part of the cycle and heals only as it begins to accelerate toward failure (Figure 8). As a result, the Ruina law generally predicts earlier susceptibility to triggering than does the Dieterich law (Figure 9). The second major difference is that for the Ruina law with small a (<0.011), transients that do not result in instantaneous failure can leave the fault slightly stronger than before, with higher state and lower velocity after the pulse has passed (Figure 8b). This is because both healing and weakening in the Ruina model are driven by slip [equation (3b)].

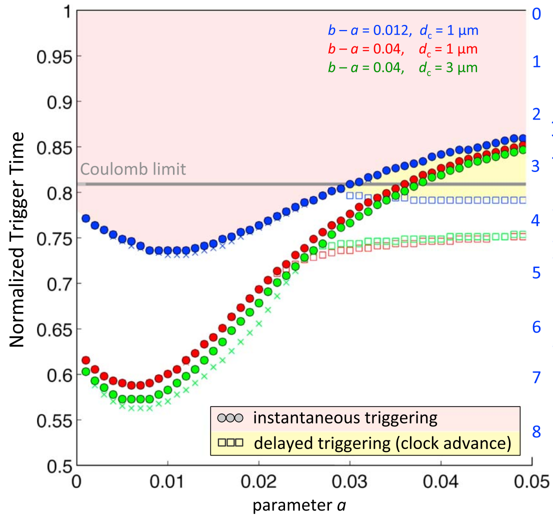

Figure 9. Onset of triggering for the Ruina slip law [equation (3b)] as a function of the rate parameter a and other model parameters. Stress pulses that arrive earlier than the open squares have negligible effect on recurrence time. Pulses that arrive between the squares and circles cause clock advance (yellow). Pulses that arrive later than the circles cause instantaneous slip (red). For some model parameters, pulses cause clock delay before the onset of instantaneous triggering (crosses). The Coulomb limit (gray bar) is the point at which instantaneous triggering is expected for a simple Coulomb friction law. Shading is for the model in blue; compare to Figure 8. The modeled stress pulse is a 1 s, 1 Hz sine pulse.

Just as with the Dieterich model, the strengthening parameter a exerts the primary control on the onset of triggering. Reducing a causes triggering onset to come earlier in the cycle, and triggering can arise significantly earlier than the Coulomb limit (Figure 9). The Ruina law thus appears to be able to match the early triggering onset observed in the experiments. For increasing a, triggering comes later, and delayed triggering with clock advance appears. The rate-weakening parameter, $b - a$, is very important for the onset of triggering in the Ruina model. Increasing the rate-weakening parameter results in earlier triggering onset across all values of a (Figure 9).

The frequency dependence of triggering is also complicated for the Ruina law. For large a (greater than ~0.011), triggering onset is determined by the duration of the transient. When the total transient duration is the same, there is no frequency dependence to triggering (Figure 10a). Single-pulse transients, with duration inversely proportional to frequency, trigger progressively later in the cycle for higher frequencies (Figure 10b). Behavior in this regime is therefore similar to the Dieterich model, although with a much earlier triggering onset. For small a (less than ~0.011), we find a much different response. Here higher-frequency transients trigger earlier in the cycle, regardless of pulse duration (Figure 10). This behavior is similar to the frequency dependence observed in the laboratory experiments.

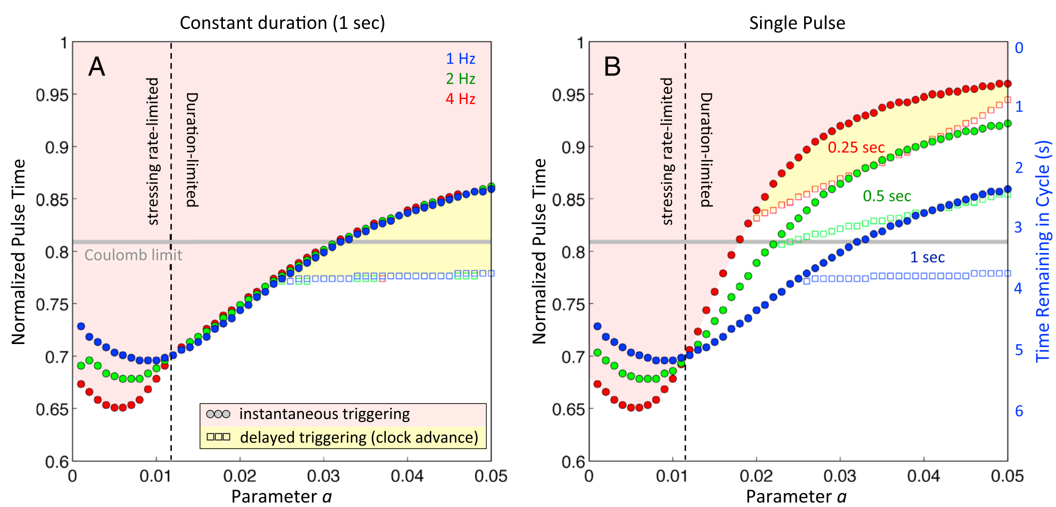

Figure 10. The effect of pulse frequency and duration for the Ruina slip law [equation (3b)]. (a) Constant-duration transients with varying frequency. Pulses that arrive below the symbols have no effect on fault slip. Pulses that arrive above the squares and below the circles cause delayed triggering with clock advance (yellow). Pulses that arrive at or above the circles cause instantaneous triggering (red). The Coulomb limit (gray bar) is the point at which instantaneous triggering is expected for a simple Coulomb friction law. Triggered response is divided into frequency-limited and duration-limited regimes. (b) Single pulse transients with varying duration. Shading is for 4 Hz, 0.25 s pulses. Model parameters: $b - a = 0.02$ and $d_c = 1$ μm.

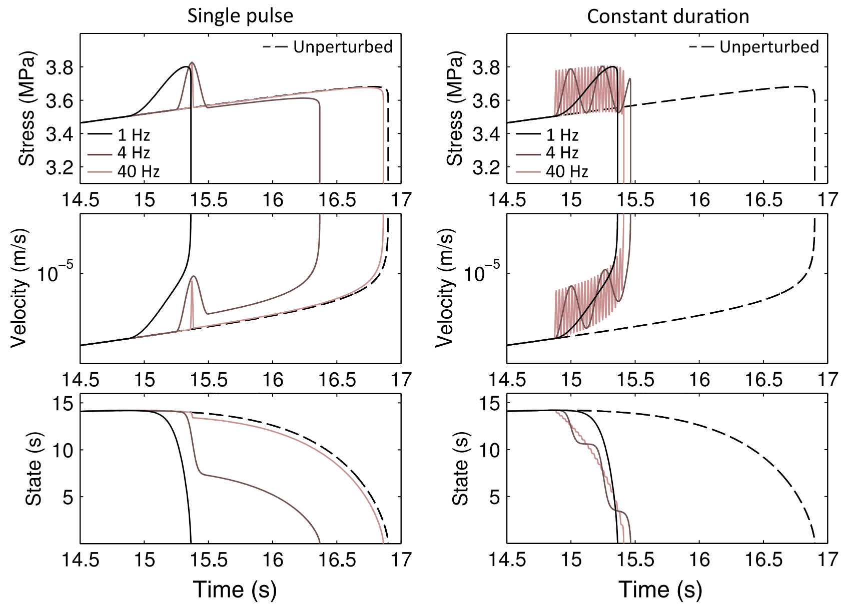

Figure 11. Frequency dependence of the slip and state response for the Dieterich aging law [equation (3a)] with $a = 0.015$. (left) Single-pulse transients are aligned on the peak of the transient. (right) Constant-duration transients are aligned on the start of the pulse. Simulation at 40 Hz shows predicted behavior at higher frequencies not tested in the experiments.

3.2.3. Mechanics of Triggering in the Rate-State Model

The laboratory experiments seem to be best matched by the Ruina slip law with small a (<0.011), based on the early onset of triggering and the positive frequency dependence. To see how different triggering behavior emerges from the models, we take a closer look at the stress, velocity, and state evolution of the slider-block models. We start with the Dieterich model for comparison, which is qualitatively similar to the Ruina law with large a (>0.011). Figure 11 shows the response to single- and multiple-pulse (constant-duration) transients of varying frequency. In both cases, delayed triggering and instantaneous triggering result from reduction of the state variable due to increased slip velocity during the transient. Instantaneous triggering occurs if the state is reduced below some critical level, and delayed triggering occurs if the state is reduced only slightly. The amount of state reduction is related to the total duration of the transient. Triggering is therefore less effective for higher-frequency, single-pulse transients but is independent of frequency for constant-duration (multiple-pulse) transients.

The Ruina law with large rate parameter ($a > 0.011$) produces triggering behavior that is qualitatively similar to the Dieterich model (compare Figures 5 and 8a). For $a < 0.011$, however, we get something quite different. The most obvious difference is that state does not immediately begin to increase and healing is somewhat delayed, compared to the other cases (Figure 8b). The slip dependence of healing in the Ruina model is at the heart of the positive frequency dependence of triggering. The basic explanation for the frequency dependence is as follows: A transient load drives an increase in sliding velocity on a weak fault. This slip results in an increase in state (healing), which resists any additional velocity increase. For low-frequency pulses, with long rise time, the state variable has plenty of time to adjust to the transient stress, and the ultimate rise in velocity is limited by healing (Figure 12). In this case, the transient produces a small decrease in stress, an increase in state, and a substantial drop in sliding velocity after the transient has passed. For high-frequency pulses with short rise time, however, the state has little time to evolve, and the peak sliding velocity can reach much higher values. The peak sliding velocity during the transient therefore ends up strongly dependent on the rise time, or stressing rate, of the transient pulse.

3.2.4. Evidence for Delayed Healing in the Experiments

The early triggering in the Ruina model (relative to the Dieterich model or the Coulomb limit) is a result of the delayed fault healing during the early part of the stick-slip cycle. In contrast to the Dieterich aging model for state evolution, a fault governed by the Ruina slip law does not begin to heal until it starts to slip. Is there additional evidence of this delayed fault healing in the experiments?

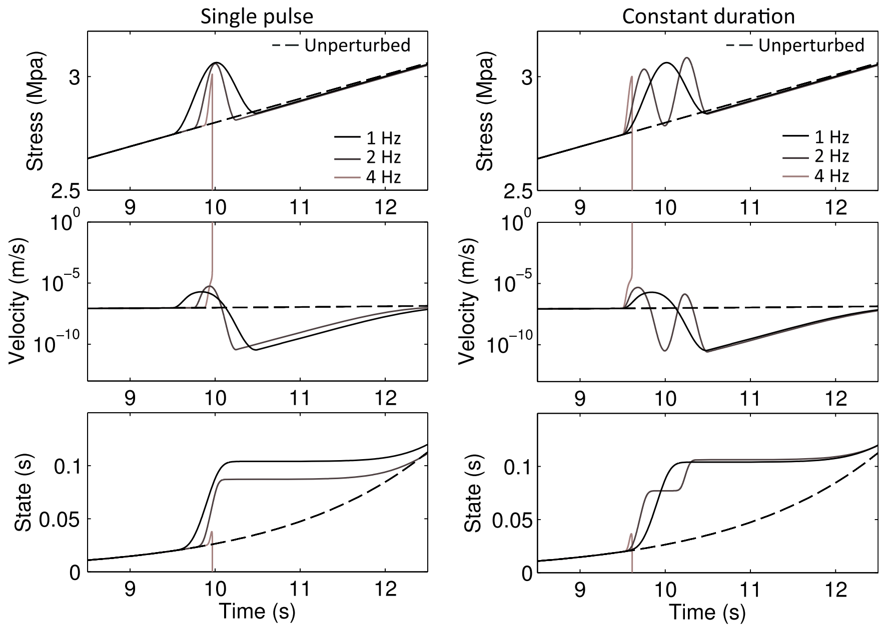

Figure 12. Period dependence of the slip and state response for the Ruina slip law [equation (3a)] with small $a = 0.005$ and $b - a = 0.03$. Low-frequency transients with long rise drive more healing (state increase, bottom panels), which limits the peak velocity. Conversely, higher-frequency pulses drive higher slip rates which lead to triggering. For transients that do not trigger instantaneously, the fault is left stronger than before with lower sliding velocity. (left) Single-pulse transients are aligned on the peak of the transient. (right) Constant-duration transients are aligned on the start of the pulse.

The modeling with the Ruina slip law with $a < 0.011$ predicts that a transient pulse should cause a small stress relaxation and a drop in sliding velocity after a mid-cycle transient. This reflects both the initially weak state and the healing that occurs during transient slip (Figures 8b and 12). The Dieterich law predicts no response, because the fault heals with time and is already strong. The experimental response to a mid-cycle transient can therefore be used to distinguish between the two state evolution laws. The experimental data for the granite surfaces show significant stress relaxation during the transient, and a reduction in slip rate after the transient has passed (Figure 13). The agreement between model and experiment is not perfect, but

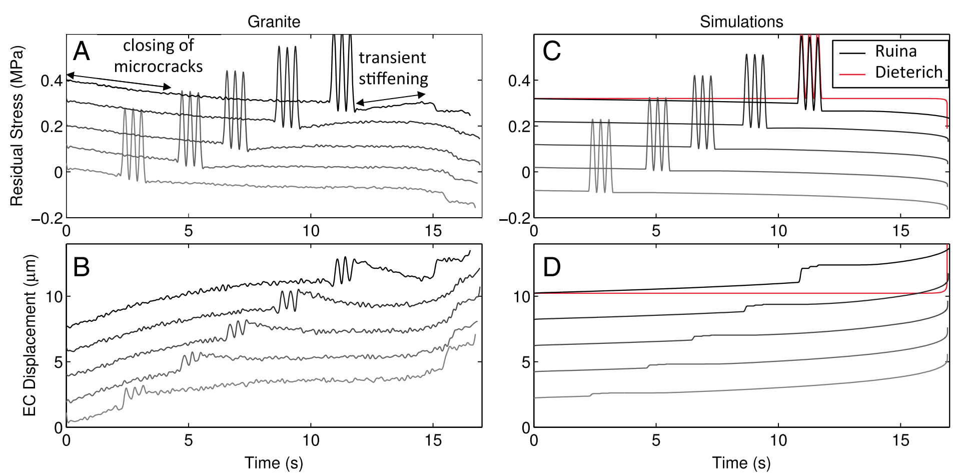

Figure 13. Stress and slip response to mid-cycle transients for granite blocks. (a) Experimentally observed stress residual, corrected for a loading frame stiffness of 250 MPa/cm load point displacement. Curves are offset for clarity. (b) Displacement of the sliding surface that would account for the stress residual. The apparent reversal of sliding velocity after the transient indicates stiffening of the system in addition to velocity reduction. (c) Simulated stress residual for rate-state models. Only one example is given for the Dieterich model for the latest pulse (red); earlier pulses produce similarly flat curves. (d) Simulated displacement. Curves are flatter after the transient than before, reflecting the post-transient reduction in sliding velocity.

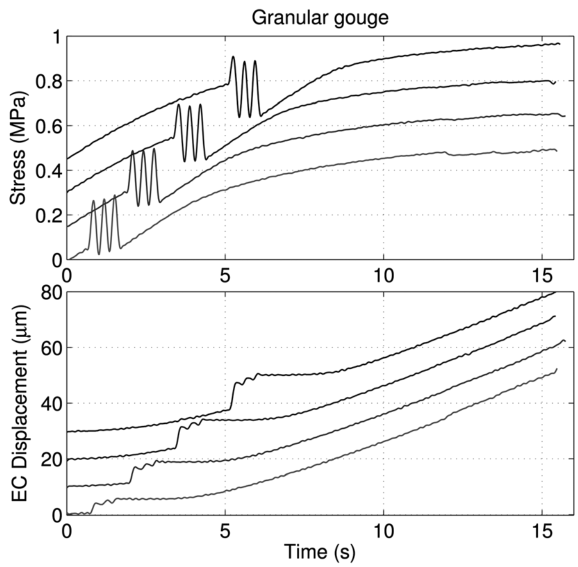

Figure 14. Stress and slip response to mid-cycle transients for granular gouge. (a) Uncorrected stress. Curves are offset for clarity. (b) Displacement of the sliding surface assuming a loading stiffness of 190 MPa/cm load point displacement. Temporary steepening of stress curve and flattening of displacement curves after the transients demonstrate slip, healing, and reduced slip rate after the transient.

the data strongly support the Ruina slip law with small $a < 0.011$. The syn-transient displacement and post-transient stiffening are even more obvious for the granular medium (Figure 14).

The experimental observations show several features not captured by the model. In the early part of the cycle, the system stiffens due to closure of microcracks, and the elastic-corrected displacement does not entirely reflect sliding. After a transient, the loading stiffness appears to increase temporarily, leading to an apparent reversal in the elastic-corrected displacement (stress is increasing faster than can be explained by the load point displacement alone). Without a displacement transducer mounted at the sliding surface itself, we cannot completely disentangle sliding velocity changes from stiffness changes. Nevertheless, the observations strongly favor the Ruina model in which healing is linked to slip, such that faults remain relatively weak throughout much of the cycle.

4. Discussion

4.1. Key Experimental Observations

There are four key features of triggering in the laboratory experiments that place constraints on the friction models. (1) Delayed triggering occurs even on bare granite surfaces. (2) The onset of triggering is much earlier than predicted by the quasi-static Coulomb friction. (3) Triggering onset is earlier for higher-frequency transients, even when the total duration of the transient is shorter. (4) In the granular medium, delayed triggering is independent of timing in the seismic cycle. The first feature, delayed triggering, is explained well by the rate-state model with either state evolution law, as long as $a > 0.02$–0.025, depending on the model. The second and third features can be explained only by the Ruina state evolution model with parameter $a < 0.011$. For this parameter range, however, the Ruina law predicts no delayed triggering, pointing to an inconsistency in the model. Finally, no choice of state evolution law or parameter range can explain delayed triggering that is independent of timing of the transient within the stick-slip cycle, of the kind seen for the granular gouge.

In the following discussion, we further analyze the source of the frequency dependence and early onset of triggering in the rate-state friction models (Features 2 and 3). We identify key slip-rate thresholds in the rate-state equations that control the qualitative features of the triggered response. These thresholds explain why delayed triggering and frequency-dependent triggering cannot occur simultaneously in the rate-state model, leaving Feature 1 incompatible with Feature 3. Finally, we scale the thresholds to fault loading timescales in order to make predictions for earthquake triggering in nature.

4.2. Healing and Weakening Thresholds in the Ruina Model

The frequency or stressing rate dependence of triggering in the Ruina model with small $a < 0.011$ is a result of the fundamental tradeoff between healing and weakening during transient slip. Examination of equation (3) for state evolution shows that the difference between weakening and healing depends on whether the transient slip velocity exceeds the weakening threshold set by

$$v_\theta = \frac{d_c}{\theta}. \tag{6}$$

For $v < v_\theta$, the state increases, while for $v > v_\theta$, the state decreases. Equation (6) defines a weakening threshold in terms of the slip rate driven by the transient; the weakening threshold must be exceeded in order to have either delayed or instantaneous triggering.

The weakening threshold v_θ is a necessary condition for triggering of any kind. For failure to occur during the transient, though, the state must weaken significantly. The displacement scale for significant weakening is the critical slip distance d_c [*Dieterich*, 1979]. For the Ruina law, this is also the length scale for significant healing. We can express this displacement requirement in terms of a second velocity threshold—the velocity at which a slip distance of d_c is covered within the duration of the transient t_{osc}.

$$v_t \sim \frac{d_c}{t_{osc}}. \tag{7}$$

We call this the slip threshold. If the slip threshold v_t is met, but not the weakening threshold v_θ, only healing can occur (perhaps leading to clock delay). Only when both thresholds are exceeded simultaneously can instantaneous triggering occur. The triggered response therefore depends on the peak slip rate during the transient, as well as the order in which the thresholds are exceeded.

The peak transient slip rate v_{max} is bounded by

$$v_{max} = v_1 \exp\left(\frac{\Delta\tau}{a\sigma}\right), \tag{8}$$

where v_1 is the background sliding velocity at the onset of the transient ($v_1 << v_{lp}$) and $\Delta\tau$ is the peak amplitude of the stress transient. Equation (8) is the peak slip rate that would be achieved if there was no evolution of state and is exact for very rapid-onset transients [equation (1)]. Equation (8) explains the first-order impact of the rate parameter a on the onset of triggering. If a is small, the change in sliding velocity during the transient must be large in order to balance the transient load. For smaller a, the transient velocity change can more easily exceed the weakening and slip thresholds v_θ and v_t.

The order in which the two velocity thresholds are met determines the triggering regime (Figure 15). If the velocity first approaches the slip threshold v_t, the actual peak slip rate will be limited by healing early in the transient. Only very rapid-onset (high stressing rate) transients will reach the peak velocity in equation (7) and reach the weakening threshold v_θ to cause instantaneous triggering. If the weakening threshold v_θ is met before the slip threshold v_t, the peak slip rate does not depend on stressing rate, because it is not limited by healing. Figure 15 shows examples where the amplitude of the stress transient is the same, but the value of a differs. The a parameter controls the duration of the cycle over which the different styles of triggering are possible, but whether triggering is actually achieved also depends on transient amplitude.

4.3. Exclusivity of Stressing Rate Dependence and Delayed Triggering

We can now explain why a rate-state slider cannot simultaneously show delayed triggering and stressing rate-dependent triggering. For delayed triggering to occur, the weakening threshold must lie below the slip threshold; $v_\theta < v_t$ (Figure 15a). For stressing rate-dependent triggering to occur, the weakening threshold must lie above the slip threshold; $v_\theta > v_t$ (Figure 15b). These two phenomena are therefore mutually exclusive. This also explains why stressing rate-dependent triggering is not observed with the Dieterich law. Under the Dieterich law [equation (3a)], the state θ increases approximately linearly with time during the early phase of the stick-slip cycle. Comparing equations (6) and (7), it is clear that stressing rate-dependent triggering ($v_\theta > v_t$) implies $\theta < t_{osc}$. This makes for a very narrow window of opportunity for stressing rate-dependent triggering under the Dieterich law.

4.4. State Weakening and Delayed Triggering (Clock Advance)

As a final point, we address the relationship between state reduction and delayed triggering (clock advance). Inspection of the weakening threshold v_θ shows that if state decreases, the velocity required to reach the weakening threshold increases proportionally. How then does a decrease in state leave the fault closer to failure?

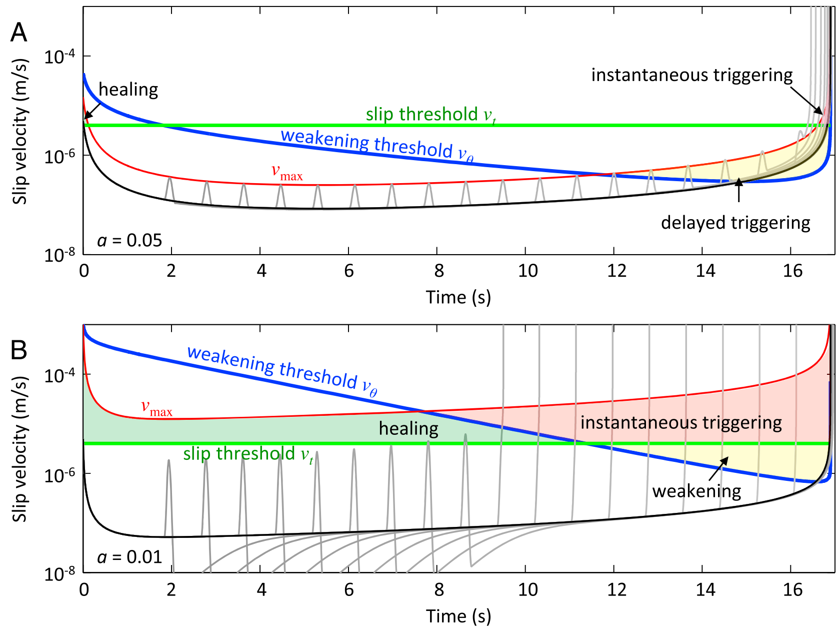

Figure 15. Summary diagrams of two regimes of triggering for the Ruina law. Gray lines show the evolution of slip velocity in simulated triggering experiments (compare to Figure 8). Triggering style depends on whether the peak transient slip rate v_{max} [red line, equation (8)] exceeds one or both of the threshold lines (blue and green). The weakening threshold v_θ [equation (6), blue line] is the slip rate above which triggering of any kind is possible. The state evolution threshold or slip threshold v_t [equation (7), green line] is the slip rate above which significant slip accumulates during the transient and instantaneous triggering is possible. (a) For large a, the weakening threshold v_θ (blue line) is met before the slip threshold v_t (green line). Peak slip rate (red) is not limited by state evolution, and delayed triggering (clock advance) is possible. (b) For small a, the slip threshold v_t is met before the weakening threshold v_θ, and the peak slip rate is limited by healing (green). The maximum slip rate (red) can be reached only if the rise time of the transient is small, causing triggering onset to be stressing rate dependent. The transient velocity increase itself is much larger for small a [equation (8)].

The answer is that any change in state must be balanced by an opposite change in the sliding velocity after the transient has passed, in order to satisfy equation (1). Assuming zero net stress change before and after the transient, the new velocity will be given by

$$v_2 = v_1 \left(\frac{\theta_1}{\theta_2}\right)^{b/a}, \tag{9}$$

where the subscripts 1 and 2 refer to before and after the transient, respectively. A decrease in state always leads to an accompanying increase in the background sliding velocity (as long as $b/a > 0$). Furthermore, the velocity increase is guaranteed to more than counteract the decrease in state, as long as the requirement for stick-slip motion is met ($b/a > 1$). Dividing both sides of equation (9) by the ratio of states (the term in parentheses) gives

$$v_2\theta_2 = v_1\theta_1 \left(\frac{\theta_1}{\theta_2}\right)^{b/a-1}. \tag{10}$$

A state decrease always results in an increase in the state-velocity product $v\theta$, if $b/a > 1$, moving the fault closer to the weakening threshold v_θ. Accordingly, a state increase during the transient results in a decrease in $v\theta$ that moves the fault farther from failure.

4.5. Discrepancies Between Model and Experiment

4.5.1. Reconciling Stressing Rate Dependence With Delayed Triggering

While the Ruina model reproduces the stressing rate dependence observed in the experiments and can also reproduce delayed triggering, it cannot do both simultaneously. It is not clear at present how to reconcile the fact that both delayed triggering and stressing rate dependence are clearly present in the experiments.

A possible solution may reside in a two state-variable friction law. This could allow the critical slip distance required for developing an instability (nucleation) to be different than the threshold for initiating the instability (triggering). However, it is not obvious that this should resolve the discrepancy, because simply changing the relative positions of the threshold lines in Figure 15 does not resolve the basic incompatibility that exists in the Ruina model.

Another possibility is that d_c is not constant throughout the cycle and in fact evolves with slip late in the cycle. If the population of contacts has a distribution of sizes, with larger contacts being stronger and longer lasting, perhaps the average size of the remaining asperities increases as the total area of real contact diminishes toward the end of the nucleation phase. This could result in the larger asperities "catching" the fault after it is weakened by a transient load, resulting in a slight delay with respect to the transient.

It is also possible that delayed triggering in the stressing rate-limited regime is a product of the temporary increase in loading stiffness after the transient (Figure 13), or some other asperity-scale process that is not captured by the friction models. [*Nagata et al.*, 2012] suggested a modification to the Dieterich aging law that reflects brittle "peeling off" of asperities under step changes in the shear stress. Some kind of stressing rate-dependent transition in the mode of asperity deformation seems like a likely candidate for explaining the results. To this end, we also ran simulations using the Nagata state evolution law. We found that while the Nagata modification can produce stressing rate-dependent triggering if the stress-weakening parameter is large enough, it does so at the expense of delayed triggering. Reconciling the observations of early-onset and stressing rate-limited triggering with the observations of delayed triggering remains beyond the scope of this paper.

4.5.2. Delayed Triggering in Granular Media

The last major feature that cannot be explained by the rate-state models is the triggered clock advance in the granular medium. The rate-state models predict that when delayed triggering and clock advance occur, they should show up in the last 10% of the cycle before the onset of instantaneous triggering. This is exactly what is observed for the granite blocks (Figure 3). For the granular gouge, a high stressing rate transient can trigger the same amount of clock advance at any time in the seismic cycle, prior to the onset of instantaneous triggering (Figure 4). We cannot readily explain this feature. Just as for the granite blocks, the delayed triggering in the granular medium may have something to do with the temporary stiffening caused by the transient pulse (Figure 14). That being said, friction in granular material involves highly anisotropic networks of grain contacts and is therefore likely to have a more complicated response to transients than bare granite surfaces.

4.6. Implications for Earthquake Triggering in Nature

The experiments on bare granite surfaces show that delayed triggering of earthquakes by transient stresses can arise as a basic consequence of frictional dynamics. This result has been anticipated by numerical treatments of rate-state friction models [*Gomberg et al.*, 1997; *Perfettini et al.*, 2003] but has not previously been demonstrated experimentally for either smooth granite surfaces or granular media.

The stressing rate dependence of triggering found in these experiments presents a challenge to conventional thinking about the insensitivity of faults to high-frequency transients [*Scholz*, 1998]. We identify two triggering regimes in the numerical models, which we term the duration-limited and the stressing rate-limited regimes. For the Dieterich model, or the Ruina model with large a ($>$0.011), we have duration-limited triggering, in that it is the total duration of the seismic transient that determines the magnitude of the triggered response. This is because weakening is cumulative across multiple oscillation cycles. This insight is supported by some suggestions of duration-dependent triggering in nature [*Pollitz et al.*, 2012].

For the Ruina slip law with small a, we have a regime in which triggering onset is frequency or stressing rate dependent. Shorter-period transients have a greater stressing rate, drive higher transient slip velocity, and hence reach the weakening threshold v_θ [equation (6)] earlier in the cycle. If the transient period (duration) is too short, though, the slip threshold v_t will not be satisfied [equation (7)], and triggering will be less effective with decreasing period. For our idealized single-pulse transient, in which rise time is inversely proportional to duration, the most effective trigger is thus the shortest pulse (oscillation period) that still satisfies the slip threshold. Whether stressing rate-limited triggering is relevant for earthquakes is critically dependent on how this optimal period scales to fault conditions.

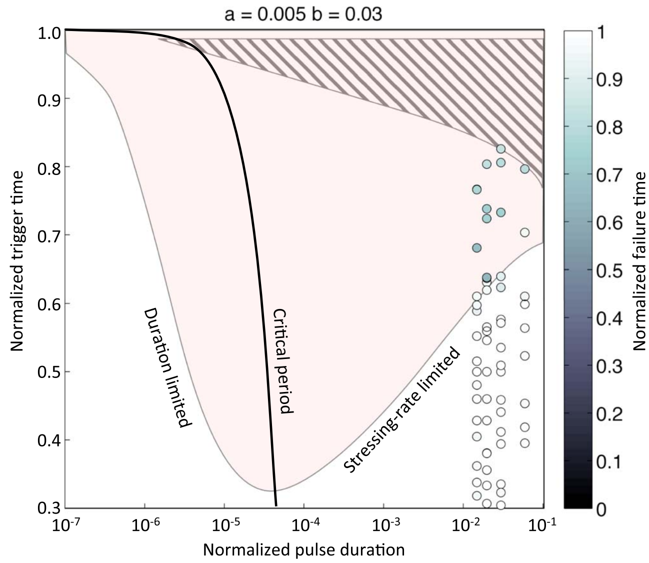

Figure 16. Onset of instantaneous triggering for single-pulse transients, as a function of duration normalized to cycle recurrence time [equation (12)]. Ruina slip law (pink) and Dieterich aging law (hatched). Parameters are $a = 0.005$ and $b = 0.03$ chosen to fit the experimental points for granite (circles). The critical period [equation (12)] separates duration limited from frequency- or stressing rate-limited triggering in the Ruina model.

4.6.1. Scaling the Triggering Thresholds to Natural Faults

In the previous section, we defined the slip threshold in terms of an approximate velocity at which sufficient slip accumulates during a transient of specified duration [equation (7)]. We can rearrange this equation to give the critical duration while specifying the velocity. Rather than use equation (7) directly, we return to the more precise definition given by equation (5). Recall that equation (5) gives the timescale for state evolution on a stably sliding interface and defines the period at which the resonant response to a continuous oscillation should be maximal [*Perfettini and Schmittbuhl*, 2001]. By inspection of the numerical simulations, we find that this equation also defines the critical timescale for triggering in stick slip, once the load point velocity is replaced by the instantaneous sliding velocity. (In a stably sliding experiment, these velocities are approximately equal.) Substituting the peak instantaneous velocity [equation (8)] into equation (5) gives

$$t_c = 2\pi\sqrt{a/(b-a)}\,\frac{d_c}{v(t)}\exp\left(-\frac{\Delta\tau}{a\sigma}\right). \tag{11}$$

To scale this equation, we first nondimensionalize the velocity by the loading rate v_{lp} and normalize the timescales (including the state variable) by the cycle recurrence time $t_r = \delta/v_{lp}$, where δ is the slip in one earthquake cycle. Keeping stress drop, peak transient stress, and other frictional parameters fixed, the triggered response then depends only on the fractional duration of the transient pulse relative to the recurrence time (Appendix B). Equation (11) becomes

$$\tilde{t}_c = 2\pi\sqrt{a/(b-a)}\,\frac{d_c}{\delta}\,\frac{1}{\tilde{v}(\tilde{t})}\exp\left(-\frac{\Delta\tau}{a\sigma}\right), \tag{12}$$

where the tilde indicates normalized values.

Figure 16 shows the shape of the triggering onset as a function of normalized period, for the experimental conditions with $a = 0.005$ and $b - a = 0.03$ (other parameters as in Table 2.) (This value of $b - a$ is well constrained by the experimentally observed triggering onset times at long relative period, but the absolute value of a is not.) The critical period t_c [equation (11)] sets the oscillation period at which triggering first appears for single-pulse transients (Figure 16). Later in the cycle, the range of periods capable of triggering expands in both directions around the critical period. Below the critical period, triggering onset is duration limited, and shorter pulses are only able to trigger later in the cycle. Above the critical period, triggering onset is frequency or stressing rate limited, and higher-frequency, shorter-duration pulses produce earlier triggering onset. Triggering is always duration limited for the Dieterich model.

The critical period [equation (11)] is not a constant and changes over the cycle as the baseline sliding velocity accelerates toward failure. The critical period is also strongly dependent on the amplitude of the stress transient, normalized by $a\sigma$. For our lab conditions at 90% of the cycle and $\Delta\tau/a\sigma \approx 10$, the critical period is ~10^{-5}, or ~169 μs in absolute terms. This prediction cannot be explored with the current experiments but will be interesting to test in the future.

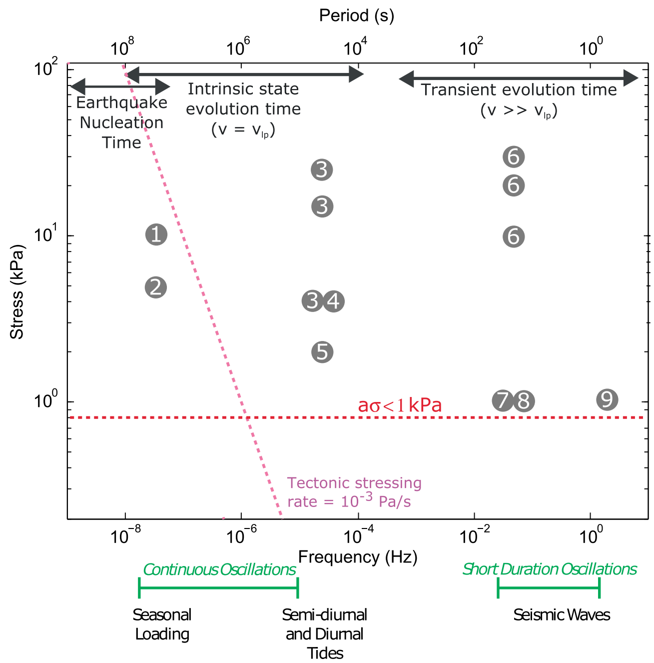

Figure 17. Schematic of triggering thresholds. Observational constraints are shown in circles; numbers indicate the study. (1) *Bollinger et al.* [2007]; (2) *Heki* [2003]; (3) *Cochran et al.* [2004]; (4) *Métivier et al.* [2009]; (5) *Stroup et al.* [2007]; (6) *Prejean et al.* [2004]; (7) *van der Elst and Brodsky* [2010]; (8) *Rubinstein et al.* [2009]; (9) *Fischer et al.* [2008]. Red line shows the lower limit for triggering observations, along with the interpreted minimum value of $a\sigma$.

Scaling the normalized critical period to natural faults requires that d_c/δ be roughly the same between earthquakes and laboratory stick slip. The laboratory value is ~85, which is appropriate for a fault with typical slip of 1 m only if natural d_c is about 1 cm. The critical period depends most strongly on the nondimensional stress $\Delta\tau/a\sigma$, because this drives the transient increase in sliding velocity. Scaling the laboratory case of $\Delta\tau/a\sigma = 10$, with $d_c/\delta = 100$, recurrence time $t_r = 30$ years, and assuming a normalized background slip rate $\tilde{v} = 0.10$ (corresponding to the Ruina model at about 90% of the cycle), we get a critical period on the order of a few hours.

If $a\sigma$ is considerably smaller, such that the nondimensional stress $\Delta\tau/a\sigma \sim 50$, the normalized critical period will be a negligible fraction of the recurrence time ($t_c \sim 10^{-23}$), and triggering will be stressing rate dependent (positively scaling with frequency) over the entire range of seismic frequencies.

On the other hand, if $a\sigma$ is significantly higher, such that the nondimensional stress $\Delta\tau/a\sigma \sim 1$, the critical period at 90% of the seismic cycle will be on the order of a year. In this case, triggering will be duration limited over the entire range of seismic (or tidal) frequencies, and short-period transients should not cause triggering except perhaps in the very late stages of nucleation when the sliding rate becomes large.

The nondimensionalization also implies that a transient of a fixed duration (such as a 20 s surface wave train) should be more effective at triggering a more rapidly loaded fault because the transient duration is longer with respect to total cycle time. This suggests that active margins, short recurrence-time seismogenic patches within creeping segments of a fault, and faults undergoing accelerated postseismic loading should all be more susceptible to triggering than more slowly loaded faults. This dependence on total cycle time may also partially explain why tectonic tremor and low-frequency earthquakes are strongly sensitive to transient forcing. The transition from seismogenic to aseismic slip may reflect a switch to velocity strengthening friction with increasing temperature, stress, or fault maturity [*Scholz*, 1998; *Wong and Zhao*, 1990]. If this frictional transition causes a decrease in recurrence time (or slip per event), it could also promote greater sensitivity to transient forcing [equation (11)]. The highly triggerable low-frequency earthquakes that constitute tectonic tremor certainly have recurrence intervals far smaller than that of a typical earthquake fault [*Shelly and Hardebeck*, 2010; *Wech and Creager*, 2011].

4.6.2. Observational Constraints on the Critical Period

There have been many observations of earthquake triggering by transient stresses, and estimates of triggering thresholds show some evidence for frequency and duration dependence in nature (Figure 17). Correlation between tides and earthquakes has been shown for stress amplitudes of 4 kPa or larger [*Cochran et al.*, 2004; *Métivier et al.*, 2009], although stresses as low as 2 kPa have produced correlations at mid-ocean ridges [*Stroup et al.*, 2007; *Wilcock*, 2001]. Seasonal loading related to snowpack and rainfall has modulated seismicity rates in Japan and the Himalaya at stresses of 5–10 kPa [*Bollinger et al.*, 2007; *Heki*, 2003]. Triggering by seismic waves on the other hand has been observed at or below 1 kPa [*Fischer et al.*, 2008; *Prejean et al.*, 2004; *Rubinstein et al.*, 2009; *van der Elst and Brodsky*, 2010], where seismic strain is estimated from peak ground velocity (1 kPa corresponds to ~0.1 mm/s PGV). Seismic waves with more energy in the lower-frequency bands (above 20 s period) have been more reliably observed to trigger seismicity [*Brodsky and Prejean*, 2005; *Gomberg and Davis*, 1996]. All of these observations require very low values of $a\sigma$.

The observations that seismic waves trigger earthquakes at stresses somewhat lower than (or comparable to) tides suggest that the critical period, at least for triggerable faults, lies somewhere below 1 day.

We have scaled equation (11) for faults with a constant ratio of earthquake slip δ to critical slip distance d_c. We used a factor of 100, which for a typical earthquake slip of 1 m corresponds to $d_c = 1$ cm. Whether this value is appropriate for faults is not well constrained. For bare-rock surfaces, d_c should increase with surface roughness [*Marone*, 1998] but remain significantly below 1 cm. In gouge zones with significant cataclastic flow, d_c should scale with gouge layer thickness. However, if deformation localizes into thin layers during earthquakes [*Marone and Kilgore*, 1993], or if smooth bare-rock asperities with small d_c dominate fault strength, d_c could more closely resemble laboratory values, increasing the ratio of fault slip to critical slip distance dramatically. In this case, the critical period [equation (11)] could be drastically reduced. If $d_c = 1$ μm as in the lab, then the normalized critical period would be 10^4 times shorter than we have estimated in this discussion, and triggering at seismic frequencies would be possible even down to a nondimensional stress of $\Delta\tau/a\sigma \sim 0.1$.

5. Conclusions

We have identified delayed triggering with clock advance, in laboratory experiments on bare granite surfaces undergoing stick-slip sliding. This shows that delayed triggering can arise from basic frictional mechanics; secondary triggering processes may not be required to explain delayed triggering of earthquakes in nature.

The lab experiments also show that the onset of triggering is earlier for higher-frequency pulses, regardless of the duration of these pulses. Triggering onset in the experiments is much earlier in the cycle than expected for a simple Coulomb threshold model of friction. The rate-and-state friction model can explain some of the observations but only in a relatively narrow model space. Specifically, the observations require the Ruina slip law for state evolution, with a rate parameter $a < 0.011$. The implication is that the laboratory faults do not heal significantly in the absence of slip, making them susceptible to triggering by moderate-amplitude high-frequency transients relatively early in the seismic cycle.

More generally, the rate-state friction model predicts two qualitatively different triggering regimes. (1) For the Dieterich state evolution law or the Ruina law with large a, triggering is duration limited. Triggering is caused by state reduction (weakening) during transient slip, and the difference between delayed and instantaneous triggering is determined by the total duration of the transient, regardless of the oscillation frequency. (2) For the Ruina law with small a, triggering is stressing rate limited and involves a competition between healing and weakening during transient-driven slip. Transients with higher stressing rate (shorter rise time) allow less healing and reach higher slip rates. Triggering occurs when a critical slip rate threshold is exceeded. In this regime, a transient that does not cause instantaneous failure leaves the fault stronger than it was before the transient.

The two triggering regimes are separated by a critical pulse duration/period that is equivalent to the natural frequency of the spring-slider system. Transient pulses at the critical period are capable of triggering a fault earliest in its seismic cycle. Observations of dynamic triggering in nature place the critical period somewhere below 1 day.

Inconsistencies remain between the model and experiments. The first is the coexistence of delayed triggering and stressing rate-limited triggering. These features are mutually exclusive in the simple rate-state model explored here. Additionally, for granular media, delayed triggering occurs regardless of when the transient occurs in the seismic cycle. This is likely related to more complicated granular dynamics than can be captured by the simple rate-state model.

The experiments and numerical simulations suggest that high-frequency, short-duration transients, such as seismic waves, could be more effective at triggering fault slip than previously recognized. This behavior emerges only in the transient response of a fault undergoing stick-slip sliding and must be modeled with the full nonlinear frictional constitutive equations, explaining why it has so far gone unnoticed. Importantly, the commonly used approximations of the Dieterich aging law, in which state goes as time since last failure, may drastically overestimate the rate of healing far from steady state and underestimate the importance of elasto-dynamic interactions between faults.

Appendix A: Fitting Rate-State Parameters to Stick-Slip Experiments

We compare the physical experiments to numerical simulations of the elastic-coupled rate-state equations [equations (1)–(3)]. The numerical models must reproduce the observed recurrence time and stress drop of the unperturbed experiments, in order for the model to be consistent with the experiments. The simplest way to achieve this for any combination of rate-state parameters is through an appropriate choice of initial conditions. Although it is possible to find non-unique combinations of *a*, *b*, and other parameters that reproduce the observed stress drop and recurrence interval in multiple stick-slip cycles, the stress drop in the experiments is likely related to processes not captured entirely by rate-state friction. It is therefore appropriate to use the observed stress drop as a constraint on the initial conditions and explore triggered stick-slip response over a full range of *a* and *b* parameters. Note that this also removes the need for an explicit damping coefficient to keep the solution stable across multiple stick slips.

This simulation technique gives results comparable to what would be obtained for a full-cycle simulation with radiation damping, as long as the recurrence interval is matched (Figure A1). This shows that the initial conditions for each stick-slip cycle are adequately specified by the stress drop in the previous slip event.

To efficiently calculate the initial stress that corresponds to a target recurrence time t_T and stress drop, we adopt an iterative approach: (1) Make a guess for the initial stress τ_0, for instance the steady state stress $\tau_* = \mu_* \sigma$ minus the target stress drop. (2) Numerically solve the coupled ODEs in equations (1)–(3) to compute the failure time t_F, given the initial stress. (3) Make a new guess for the initial stress τ_0' based on the difference between the computed and target recurrence times and the loading rate $\dot{\tau}$,

$$\tau_0' = \tau_0 - (t_T - t_F)\,\dot{\tau} \tag{A1}$$

(4) Return to step 2 until the correction to the starting stress in equation (A1) falls below some small value. This approach converges to within 10^{-3} s of the target recurrence time in a few iterations. We use the Matlab ODE solver ode15s to run the simulations. We define the ultimate failure time t_F as the point at which the state variable reaches a value of 10^{-4} from above.

If we take the initial stress τ_0 as the minimum stress in the stick-slip cycle, where $\dot{\tau} = 0$, then the initial velocity $v_0 = v_{lp}$ [equation (2)]. The initial state θ_0 is then uniquely defined by equation (1).

When using the Dieterich aging model (3a), the velocity can approach very small values, resulting in numerical rounding errors. We therefore take advantage of an approximation. At the very beginning of the cycle, we assume that the fault is fully locked and the state variable is just equal to the time since the previous slip event. At the 10% mark, we transition to a full numerical solution. This avoids round-off errors during the early portion of the loading cycle and does not affect simulations in the later portions of the loading cycle.

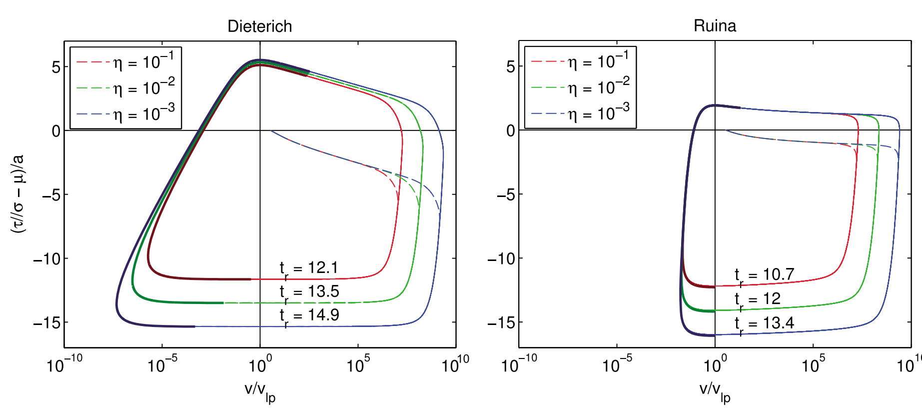

Figure A1. Full-cycle rate-state simulations including radiation damping (thin lines) and quasi-static simulations excluding radiation damping but using the recurrence time from the full simulations as a constraint on the initial conditions (the approach used in this study thick lines). Full simulations start near steady state (center) and move clockwise in a periodic stick-slip cycle. Different curves differ only by the radiation damping coefficient used to limit peak slip rate.

Appendix B: Nondimensional Weakening Threshold

Here we show that the onset of triggering, expressed as a fraction of the stick-slip cycle, is independent of the loading rate, as long as the recurrence time of the stick-slip cycle is inversely proportional to the loading rate. This is equivalent to saying that the displacement $\delta = v_{\mathrm{lp}} t_{\mathrm{r}}$ in a complete seismic cycle is independent of loading rate. This may not be strictly true in nature but is good enough for our model purposes.

To start, we nondimensionalize the rate-state equations by the substitutions

$$\widetilde{\theta} = \frac{\theta}{t_{\mathrm{r}}} \tag{B1a}$$

$$\widetilde{t} = \frac{t}{t_{\mathrm{r}}} \tag{B1b}$$

$$\widetilde{v} = \frac{v}{v_{\mathrm{lp}}}. \tag{B1c}$$

This leads to the nondimensional state evolution equation [using equation (3b)]

$$\dot{\widetilde{\theta}} = -\widetilde{\theta}\,\widetilde{v}\frac{v_{\mathrm{lp}} t_{\mathrm{r}}}{d_{\mathrm{c}}} \ln\left(\widetilde{\theta}\,\widetilde{v}\frac{v_{\mathrm{lp}} t_{\mathrm{r}}}{d_{\mathrm{c}}}\right), \tag{B2}$$

and the nondimensionalized weakening threshold

$$\widetilde{\theta}\,\widetilde{v} = \frac{d_{\mathrm{c}}}{v_{\mathrm{lp}} t_{\mathrm{r}}} = \frac{d_{\mathrm{c}}}{\delta}. \tag{B3}$$

If the displacement during one complete cycle is taken not to depend on v_{lp}, then a fault's proximity to weakening along its loading path is identical for different loading rates, when expressed as a function of the fractional time in the cycle. A transient with frequency, duration, and timing all scaled by equation (B1) will have an identical effect on the nondimensionalized velocity and state. Under this rescaling, the ratios of the transient stress to the stress drop, and of the transient duration to the cycle duration, remain constant.

Similarly, the slip threshold [equation (7)] can be rescaled as

$$\widetilde{v}\,\widetilde{t}_{\mathrm{osc}} = \frac{d_{\mathrm{c}}}{v_{\mathrm{lp}} t_{\mathrm{r}}} = \frac{d_{\mathrm{c}}}{\delta}. \tag{B4}$$

Acknowledgments
This paper benefitted from discussion with Bruce Shaw, Chris Marone, Alan Rubin, and Pathikrit Bhattacharya. Chris Scholz gave helpful remarks on an early draft of the paper. We also thank Alexandre Schubnel and two anonymous reviewers for thorough and thoughtful comments. NJvdE is supported by National Science Foundation (NSF) grant EAR-1144503. This work was also supported by Southern California Earthquake Center (SCEC) grant 13117. The experimental data for this paper are available by contacting HM Savage at hsavage@ldeo.columbia.edu.

References

Ader, T. J., J. P. Ampuero, and J. P. Avouac (2012), The role of velocity-neutral creep on the modulation of tectonic tremor activity by periodic loading, *Geophys. Res. Lett.*, *39*, L16310, doi:10.1029/2012GL052326.

Beeler, N. M., and D. A. Lockner (2003), Why earthquakes correlate weakly with the solid Earth tides: Effects of periodic stress on the rate and probability of earthquake occurrence, *J. Geophys. Res.*, *108*(B8), 2391, doi:10.1029/2001JB001518.

Belardinelli, M. E., A. Bizzarri, and M. Cocco (2003), Earthquake triggering by static and dynamic stress changes, *J. Geophys. Res.*, *108*(B3), 2135, doi:10.1029/2002JB001779.

Boettcher, M. S., and C. Marone (2004), Effects of normal stress variation on the strength and stability of creeping faults, *J. Geophys. Res.*, *109*, B03406, doi:10.1029/2003JB002824.

Bollinger, L., F. Perrier, J. P. Avouac, S. Sapkota, U. Gautam, and D. Tiwari (2007), Seasonal modulation of seismicity in the Himalaya of Nepal, *Geophys. Res. Lett.*, *34*, 332–344, doi:10.1029/2006GL029192.

Brodsky, E. E. (2006), Long-range triggered earthquakes that continue after the wave train passes, *Geophys. Res. Lett.*, *33*, L15313, doi:10.1029/2006GL026605.

Brodsky, E. E., and S. G. Prejean (2005), New constraints on mechanisms of remotely triggered seismicity at Long Valley Caldera, *J. Geophys. Res.*, *110*, B04302, doi:10.1029/2004JB003211.

Brodsky, E. E., and N. J. van der Elst (2014), The uses of dynamic earthquake triggering, *Annu. Rev. Earth Planet. Sci.*, *42*, 317–339.

Brodsky, E. E., V. Karakostas, and H. Kanamori (2000), A new observation of dynamically triggered regional seismicity: Earthquakes in Greece following the August, 1999 Izmit, Turkey earthquake, *Geophys. Res. Lett.*, *27*(17), 2741–2744, doi:10.1029/2000GL011534.

Brodsky, E. E., E. Roeloffs, D. Woodcock, I. Gall, and M. Manga (2003), A mechanism for sustained groundwater pressure changes induced by distant earthquakes, *J. Geophys. Res.*, *108*(B8), 2390, doi:10.1029/2002JB002321.

Cochran, E. S., J. E. Vidale, and S. Tanaka (2004), Earth tides can trigger shallow thrust fault earthquakes, *Science*, *306*(5699), 1164–1166.

Dieterich, J. H. (1979), Modeling of rock friction: 1. Experimental results and constitutive equations, *J. Geophys. Res.*, *84*(Nb5), 2161–2168, doi:10.1029/JB084iB05p02161.

Dieterich, J. H. (1987), Nucleation and triggering of earthquake slip: Effect of periodic stresses, *Tectonophysics*, *144*(1), 127–139.

Dieterich, J. H. (1992), Earthquake nucleation on faults with rate-dependent and state-dependent strength, *Tectonophysics*, *211*(1–4), 115–134.

Dieterich, J. (1994), A constitutive law for rate of earthquake production and its application to earthquake clustering, *J. Geophys. Res.*, *99*(B2), 2601–2618, doi:10.1029/93JB02581.

Dieterich, J. H., and G. Conrad (1984), Effect of humidity on time- and velocity-dependent friction in rocks, *J. Geophys. Res.*, *89*(B6), 4196–4202, doi:10.1029/JB089iB06p04196.

Elkhoury, J. E., E. E. Brodsky, and D. C. Agnew (2006), Seismic waves increase permeability, *Nature*, *441*(7097), 1135–1138.

Elkhoury, J. E., A. Niemeijer, E. E. Brodsky, and C. Marone (2011), Laboratory observations of permeability enhancement by fluid pressure oscillation of in situ fractured rock, *J. Geophys. Res.*, *116*, B02311, doi:10.1029/2010JB007759.

Felzer, K. R., and E. E. Brodsky (2006), Decay of aftershock density with distance indicates triggering by dynamic stress, *Nature*, *441*(7094), 735–738.

Fischer, A. D., C. G. Sammis, Y. Chen, and T.-L. Teng (2008), Dynamic triggering by strong-motion P and S waves: Evidence from the 1999 Chi-Chi, Taiwan, earthquake, *Bull. Seismol. Soc. Am.*, *98*(2), 580–592.

Gomberg, J., and S. Davis (1996), Stress strain changes and triggered seismicity at The Geysers, California, *J. Geophys. Res.*, *101*(B1), 733–749, doi:10.1029/95JB03250.

Gomberg, J., and P. Johnson (2005), Seismology—Dynamic triggering of earthquakes, *Nature*, *437*(7060), 830–830.

Gomberg, J., M. L. Blanpied, and N. M. Beeler (1997), Transient triggering of near and distant earthquakes, *Bull. Seismol. Soc. Am.*, *87*(2), 294–309.

Gomberg, J., N. M. Beeler, M. L. Blanpied, and P. Bodin (1998), Earthquake triggering by transient and static deformations, *J. Geophys. Res.*, *103*(B10), 24,411–24,426, doi:10.1029/98JB01125.

Gomberg, J., P. A. Reasenberg, P. Bodin, and R. A. Harris (2001), Earthquake triggering by seismic waves following the Landers and Hector Mine earthquakes, *Nature*, *411*(6836), 462–466.

Gomberg, J., P. Bodin, and P. A. Reasenberg (2003), Observing earthquakes triggered in the near field by dynamic deformations, *Bull. Seismol. Soc. Am.*, *93*(1), 118–138.

Gu, J. C., J. R. Rice, A. L. Ruina, and S. T. Tse (1984), Slip motion and stability of a single degree of freedom elastic system with rate and state dependent friction, *J. Mech. Phys. Solids*, *32*(3), 167–196.

Heki, K. (2003), Snow load and seasonal variation of earthquake occurrence in Japan, *Earth Planet. Sci. Lett.*, *207*(1), 159–164.

Hill, D. P., and S. G. Prejean (2007), *Dynamic Triggering*, *Treatise Geophys*., edited by H. Kanamori, Elsevier, Amsterdam.

Hill, D. P., et al. (1993), Seismicity remotely triggered by the magnitude 7.3 Landers, California, Earthquake, *Science*, *260*(5114), 1617–1623.

Husker, A. L., and E. E. Brodsky (2004), Seismicity in Idaho and Montana triggered by the Denali fault earthquake: A window into the geologic context for seismic triggering, *Bull. Seismol. Soc. Am.*, *94*(6), S310–S316.

Ikari, M. J., C. Marone, and D. M. Saffer (2011), On the relation between fault strength and frictional stability, *Geology*, *39*(1), 83–86.

Ikari, M. J., C. Marone, D. M. Saffer, and A. J. Kopf (2013), Slip weakening as a mechanism for slow earthquakes, *Nat. Geosci.*, *6*(6), 468–472.

Marone, C. (1998), Laboratory-derived friction laws and their application to seismic faulting, *Annu. Rev. Earth Planet. Sci.*, *26*, 643–696.

Marone, C., and B. Kilgore (1993), Scaling of the critical slip distance for seismic faulting with shear strain in fault zones, *Nature*, *362*(6421), 618–621.

Métivier, L., O. de Viron, C. P. Conrad, S. Renault, M. Diament, and G. Patau (2009), Evidence of earthquake triggering by the solid earth tides, *Earth Planet. Sci. Lett.*, *278*(3), 370–375.

Nagata, K., M. Nakatani, and S. Yoshida (2012), A revised rate- and state-dependent friction law obtained by constraining constitutive and evolution laws separately with laboratory data, *J. Geophys. Res.*, *117*, B02314, doi:10.1029/2011JB008818.

Peng, Z. G., D. P. Hill, D. R. Shelly, and C. Aiken (2010), Remotely triggered microearthquakes and tremor in central California following the 2010 M(w) 8.8 Chile earthquake, *Geophys. Res. Lett.*, *37*, L24312, doi:10.1029/2010GL045462.

Perfettini, H., and J. Schmittbuhl (2001), Periodic loading on a creeping fault: Implications for tides, *Geophys. Res. Lett.*, *28*(3), 435–438, doi:10.1029/2000GL011686.

Perfettini, H., J. Schmittbuhl, and A. Cochard (2003), Shear and normal load perturbations on a two-dimensional continuous fault: 2. Dynamic triggering, *J. Geophys. Res.*, *108*(B9), 2409, doi:10.1029/2002JB001805.

Pollitz, F. F., R. S. Stein, V. Sevilgen, and R. Burgmann (2012), The 11 April 2012 east Indian Ocean earthquake triggered large aftershocks worldwide, *Nature*, *490*(7419), 250–253, doi:10.1038/nature11504.

Prejean, S. G., D. P. Hill, E. E. Brodsky, S. E. Hough, M. J. S. Johnston, S. D. Malone, D. H. Oppenheimer, A. M. Pitt, and K. B. Richards-Dinger (2004), Remotely triggered seismicity on the United States west coast following the M-W 7.9 Denali fault earthquake, *Bull. Seismol. Soc. Am.*, *94*(6), S348–S359.

Rice, J., and A. Ruina (1983), Stability of steady frictional slipping, *J. Appl. Mech.*, *50*(2), 343–349.

Rubinstein, J. L., J. Gomberg, J. E. Vidale, A. G. Wech, H. Kao, K. C. Creager, and G. Rogers (2009), Seismic wave triggering of nonvolcanic tremor, episodic tremor and slip, and earthquakes on Vancouver Island, *J. Geophys. Res.*, *114*, B00A01, doi:10.1029/2008JB005875.

Rubinstein, J. L., et al. (2011), Widespread triggering of earthquakes and tremor by the 2011 M9.0 off-Tohoku earthquake, *Seismol. Res. Lett.*, *82*(2), 273–361.

Ruina, A. (1983), Slip instability and state variable friction laws, *J. Geophys. Res.*, *88*(Nb12), 359–370.

Savage, H. M., and C. Marone (2007), Effects of shear velocity oscillations on stick-slip behavior in laboratory experiments, *J. Geophys. Res.*, *112*, B02301, doi:10.1029/2005JB004238.

Savage, H. M., and C. Marone (2008), Potential for earthquake triggering from transient deformations, *J. Geophys. Res.*, *113*, B05302, doi:10.1029/02007JB005277.

Scholz, C. H. (1998), Earthquakes and friction laws, *Nature*, *391*(6662), 37–42.

Scholz, C. H. (2003), Earthquakes—Good tidings, *Nature*, *425*(6959), 670–671.

Shelly, D. R., and J. L. Hardebeck (2010), Precise tremor source locations and amplitude variations along the lower-crustal central San Andreas Fault, *Geophys. Res. Lett.*, *37*, L14301, doi:10.1029/2010GL043672.

Shelly, D. R., Z. G. Peng, D. P. Hill, and C. Aiken (2011), Triggered creep as a possible mechanism for delayed dynamic triggering of tremor and earthquakes, *Nat. Geosci.*, *4*(6), 384–388.

Stroup, D., D. Bohnenstiehl, M. Tolstoy, F. Waldhauser, and R. Weekly (2007), Pulse of the seafloor: Tidal triggering of microearthquakes at 9°50′ N East Pacific Rise, *Geophys. Res. Lett.*, *34*, L15301, doi:10.1029/2007GL030088.

van der Elst, N. J., and E. E. Brodsky (2010), Connecting near-field and far-field earthquake triggering to dynamic strain, *J. Geophys. Res.*, *115*, B07311, doi:10.1029/2009JB006681.

van der Elst, N. J., H. Savage, K. M. Keranen, and G. A. Abers (2013), Enhanced remote triggering at sites of fluid injection in the Midwestern U.S, *Science*, *341*(6142), 164–167.

Velasco, A. A., S. Hernandez, T. Parsons, and K. Pankow (2008), Global ubiquity of dynamic earthquake triggering, *Nat. Geosci.*, *1*(6), 375–379.

Wech, A. G., and K. C. Creager (2011), A continuum of stress, strength and slip in the Cascadia subduction zone, *Nat. Geosci.*, *4*(9), 624–628, doi:10.1038/NGEO1215.
Wilcock, W. S. (2001), Tidal triggering of microearthquakes on the Juan de Fuca Ridge, *Geophys. Res. Lett.*, *28*(20), 3999–4002, doi:10.1029/2001GL013370.
Wong, T.-F., and Y. Zhao (1990), Effects of load point velocity on frictional instability behavior, *Tectonophysics*, *175*, 177–195.
Wu, C. Q., Z. G. Peng, W. J. Wang, and Q. F. Chen (2011), Dynamic triggering of shallow earthquakes near Beijing, China, *Geophys. J. Int.*, *185*(3), 1321–1334.